

PLASTIC INSTABILITY AND FRACTURE IN SHEETS  
STRETCHED OVER RIGID PUNCHES

by

STUART PHILIP KEELER

A.B., Ripon College  
(1957)

S.B., Massachusetts Institute of Technology  
(1957)

Submitted in Partial Fulfillment of the  
Requirements for the Degree of

DOCTOR OF SCIENCE

at the

MASSACHUSETTS INSTITUTE OF TECHNOLOGY

May, 1961

Signature of Author

Signature redacted

Department of Metallurgy

Certified by

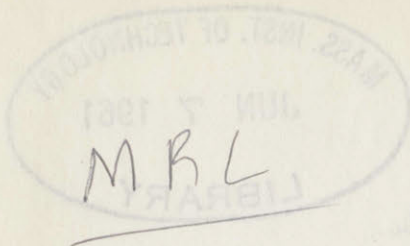
Signature redacted

Thesis Supervisor

Accepted by

Signature redacted

Chairman, Departmental Committee  
on Graduate Students



metall  
Thesis

PLASTIC INSTABILITY AND FRACTURE IN SHEETS  
STRETCHED OVER RIGID PUNCHES  
1961

by  
STUART PHILIP KEELER

A.B., Ripon College  
(1957)  
S.B., Massachusetts Institute of Technology  
(1957)

Submitted in Partial Fulfillment of the  
Requirements for the Degree of

DOCTOR OF SCIENCE

of the  
MASSACHUSETTS INSTITUTE OF TECHNOLOGY

May, 1961

*Stuart P. Keeler*  
Department of Metallurgy

Signature of Author

*Walter O. Baker*  
Thesis Supervisor

Certified by

*John V. Water*  
Chairman, Departmental Committee  
on Graduate Students

Accepted by

PLASTIC INSTABILITY AND FRACTURE IN SHEETS  
STRETCHED OVER RIGID PUNCHES

by

STUART PHILIP KEELER

Submitted to the Department of Metallurgy on April 27, 1961  
in partial fulfillment of the requirements for the  
Degree of Doctor of Science

---

ABSTRACT

Sheets were securely clamped, stretched over rigid punches, and strain distributions measured for different conditions of lubrication and punch form. In general, the development of strain in the various elements of a sheet was marked at some stage of the stretching by a discontinuous increase in  $\epsilon_p$ , the algebraically largest component. Because both principal strains were tensile everywhere in the plane of the sheet, localized necking could not occur and plastic instability appeared as "diffuse necking". The strain at the  $\epsilon_p$  discontinuity in any element was in good agreement with that predicted by theory for the beginning of unstable flow under the prevailing principal-stress ratio. With continued punch movement, the unstable region grew wider around the position where instability first occurred and where ductile fracture eventually ended the stretching. A fracture criterion of nearly constant  $\epsilon_p$  was indicated for a number of annealed materials, the critical



value of about 0.4 holding for all. Other observations revealed how fracturing was influenced by structure and processing history. It was concluded that under these conditions, the most effective method of increasing stretching limits would be the development of a more nearly uniform distribution of strain in the sheet. Factors contributing to such a distribution were shown to be a more persistent rate of material strain hardening, lower punch-sheet interface friction, and greater punch curvature. Some application to practical stamping failure-analysis has been suggested.

Thesis Supervisor: Walter A. Backofen

Title: Associate Professor of Metallurgy



## TABLE OF CONTENTS

	<u>Page</u>
ABSTRACT-----	ii
LIST OF ILLUSTRATIONS-----	vi
LIST OF TABLES-----	ix
ACKNOWLEDGEMENTS-----	x
I INTRODUCTION-----	1
II MATERIALS AND PROCEDURES-----	13
Materials-----	13
Specimens-----	17
Stretching-----	17
Lubrication-----	20
Punch Form-----	20
Strain Measurements-----	21
III RESULTS-----	23
Instability Considerations-----	27
Fracturing Considerations-----	33
IV DISCUSSION-----	46
Limit Control in Punch Stretching-----	46
Applications-----	47
V CONCLUSIONS-----	51
REFERENCES-----	53

## TABLE OF CONTENTS

	<u>Page</u>
APPENDIX A: DETERMINATION OF CONDITIONS FOR INSTABILITY-----	58
Definitions and Basic Equations-----	58
Angle of Localized Neck-----	61
Work Hardening Conditions-----	64
APPENDIX B: DETAILS OF SPECIMEN PREPARATION AND TESTING APPARATUS	70
Specimen Preparation-----	70
Apparatus and Test Procedure-----	72
APPENDIX C: ADDITIONAL SAMPLING OF STRAIN HISTORY DATA-----	75
APPENDIX D: INSTABILITY IN HYDRAULIC BULGE TESTS-----	79
APPENDIX E: FRACTURE EXAMINATION-----	80
SUGGESTIONS FOR FUTURE WORK-----	83
BIOGRAPHICAL NOTE-----	84



## LIST OF ILLUSTRATIONS

<u>Figure</u>		<u>Page</u>
1	Graphical Determination of Instability Strain in a Sheet Uniformly Loaded in Its Plane. $Z$ is a function of the principal stress ratio $\sigma_2/\sigma_1$ ( $\sigma_3 = 0$ ); $Z_d$ relates to the beginning of diffuse and $Z_l$ to the beginning of localized necking. For uniaxial tension, $\bar{\sigma} = \sigma$ , $\bar{\epsilon} = \epsilon_1$ , $Z_d = 1$ , and $Z_l = 2$ .-----	5
2	A Localized Neck at Angle $\alpha$ . No extension occurs along the neck. The angle $\alpha$ is determined by the stress ratio. For uniaxial tension in an isotropic sheet, $\alpha = 54^\circ 44'$ ; it increases to $90^\circ$ for $\sigma_2/\sigma_1 = 1/2$ ( $d\epsilon_2 = 0$ ).-----	7
3	The Development of Unstable Flow as Influenced by Stress Ratio, $X$ , and Strain-hardening Characteristics, Measured in Terms of $\beta$ (Isotropic Sheet). Deformation at constant $X$ is represented by a vertical line on the abscissa. Deformation begins at high $\beta$ , a decrease in $\beta$ indicating increased straining along stress-strain curve. For $X > 1/2$ , geometrical restrictions prevent localized necking. Development has been based on an analysis of Hill. <sup>18</sup> -----	9
4	Dependence on Plastic Anisotropy of the Limiting (Maximum) $X$ Above Which Localized Necking Cannot Occur. $R$ is the ratio of width to thickness strain in a uniaxial tension test, and equals 1 only for complete isotropy. In the plotting, $R$ has been taken to be independent of direction in the sheet (planar isotropy). Development has been based on an analysis of Hill. <sup>18</sup> -----	10
5	A Three Dimensional Representation of How Unstable Flow Develops Under Different Conditions of $X$ , $R$ , and $\beta$ . A section at $R = 1$ (isotropic sheet) is given in Fig. 3. Projection of the curve intersection (limit for localized necking) on the $X$ - $R$ plane is presented in Fig. 4. Development has been based on an analysis of Hill. <sup>18</sup> -----	11
6	True Stress vs. True Strain Curves, $0^\circ$ and $90^\circ$ to Sheet-Rolling Direction, Obtained by Tension Testing of Both As-Received Material and Specimens Prestrained by Rolling. The curves coincide in regions of overlap.-----	16
7	Dependence on Stress Ratio of Total Effective Strain, $\bar{\epsilon}_d^*$ , and Algebraically Largest Component, $\epsilon_1^*$ , for Diffuse Necking. Computed for All Test Materials by Method of Fig. 1 From Stress-strain Curves in Fig. 6. All Materials Assumed to be Isotropic for the Computation.-----	18



<u>Figure</u>		<u>Page</u>
8	Schematic of Subpress.-----	19
9	Distribution of Radial and Circumferential Strain Across the Dome for Various Pole Heights, Up to Fracture, in Teflon-lubricated, Half-hard Aluminum Stretched over a Hemispherical Punch. Failure location is indicated by vertical arrow. All measurements are plotted at radial positions locating the elements in an unstretched specimen.-----	24
10	Typical Load vs. Pole Height Record for Teflon-lubricated, Half-hard Aluminum Stretched Over a Hemispherical Punch. Note load rising steadily as instability develops. A load arrest occurs with the formation of a shear band.-----	25
11	Increase of Radial and Circumferential Strain with Pole Height at the Fracture Location in Teflon-lubricated, Half-hard Aluminum Stretched Over a Hemispherical Punch. A discontinuity at $\epsilon_r^* - h^*$ separates regions I and II. Fracture is indicated by symbol x.-----	26
12	Radial Strain vs. Pole Height in Various Elements of Unlubricated, Half-hard Aluminum Stretched Over a Hemispherical Punch. Note strain discontinuity, indicated by vertical line, occurring first at location of eventual failure, and subsequently in surrounding elements. Strain at fracture in the $r_0 = 0.60$ in. element is indicated by symbol x.-----	30
13	Increase in Pole Height, $h^*$ , as Material Adjacent to the First Unstable Element Satisfies the Diffuse-necking Condition and the Unstable Band Grows Wider. Soft and Half-hard aluminum, Unlubricated and Teflon-lubricated, Stretched Over a Hemispherical Punch.-----	31
14	Percentage of Pole Height Attained After Instability Related to the Maximum Pole Height at Fracture for All Materials and Test Conditions.-----	34
15	Distributions of Radial and Thickness Strain at the Maximum (Fracture) Pole Height for Lubricated, Soft Materials Stretched Over a Hemispherical Punch, Showing Approximately Constant Peak Strain for All Materials. Note uniformity of thickness strain in brass. All measurements are plotted at radial positions locating the elements in an unstretched specimen.-----	35

<u>Figure</u>	<u>Page</u>	
16	A Summary of All Fracture Strain Measurements. The various data are plotted against the ratio of circumferential to radial strain at fracture for all materials and test conditions. The dashed radial-strain line was computed from that drawn through the circumferential-strain points. Note the approximately constant value of radial strain for all soft materials.-----	36
17	Distributions of Radial Strain at Maximum (Fracture) Pole Height in Steel Stretched with Different Lubrication and Punch Geometry. Peak strain for HD taken just prior to localized necking does not represent actual fracture strain. Failure locations are indicated by vertical arrow. All measurements are plotted at radial positions locating the elements in an unstretched specimen.-----	38
18	Radial Strain vs. Pole Height at Various Radial Locations On Soft Aluminum Stretched Over a Hemispherical Punch. Teflon Lubricant was removed during the test. Note reduced straining at locations in contact with punch at time of lubricant removal. Strain at failure height is indicated by symbol x.-----	39
19	Photomicrographs of Fracture Regions: (a) Hard Copper-HT with Crack Forming at Intersection of Two Shear Planes; (b) Portion of Localized Neck in Steel-HD Showing Crack Forming at Surface; (c) Complete Shear Separation in Steel-HT. All Specimens were nickel-plated prior to examination.-----	41
20	Fracture in Hard Brass-HT (Specimen A) and Soft Brass-HD (Specimen B). Rolling direction is indicated by arrow; tear is encircled by dotted line. Fracture began tangential to rolling direction at a location indicated by vertical line. Grid was partially removed by cleaning and handling after testing.-----	44
1A	Components of Elongation of a Localized Neck in a Sheet Uniformly Loaded in Its Plane ( $\sigma_3 = 0$ ).-----	62
2A	Strain vs. Pole Height for Various Materials in Bulge Testing. Data were replotted from Brown and Thompson <sup>27</sup> to show straining behavior similar to punch stretching. Strain predicted for onset of instability is indicated by $\epsilon_T^*$ .-----	80
3A	Enlargement of Crack Found Along Shear Band in Hard Copper (HT). Ammonium Persulfate Etch, X300.-----	82



## LIST OF TABLES

<u>Table</u>		<u>Page</u>
I	Materials Tested-----	14
II	Plastic Anisotropy Coefficients-----	15
III	Strain History of Failure Elements-----	29
IV	Sheet Thickness Variation at Fracture Sites in Tension Specimens and Stretched Cups-----	43
IA	Strain History of Various Elements From Each Cup-----	76



## ACKNOWLEDGEMENTS

The author is indebted to Professor W. A. Backofen for suggesting the research topic, and would like to thank him for his continued guidance, criticism, encouragement, and patience. The author is also indebted to National Steel Corporation for supporting this research through a fellowship program. Great Lakes Steel Company, and in particular Mr. C. L. Altenburger, are to be thanked for their direct and constant interest in the work. The author also wishes to express his appreciation to Professor G. Pearsall for the many discussions concerning the theoretical aspects of this work, Mr. R. H. Foss and Mr. R. L. Jones for assistance in building the experimental apparatus.

## I. INTRODUCTION

The problem of defining, measuring, and controlling workability is found in all kinds of deformation processing. A common basis for the difficulty in attempting to cope with it is uncertainty about conditions that distinguish the actual processing operation. An especially involved example is found in the drawability of sheet; like others, it may be subdivided into a few interrelated parts. One such part is radial drawing as represented by the wedge-draw test<sup>1,2</sup> and studied in great detail by Chung and Swift<sup>3</sup> as it occurs, with bending, in the conversion of a circular flange into the wall of a cylindrical cup. Another, the subject of this paper, is stretching over a punch of fixed geometry with friction in the punch-sheet interface -- described as punch-stretching in the discussion to follow. Still others, classed here as lesser sub-problems, are bending alone, compression (shear) cracking in flanges, buckling or wrinkling, resulting surface control, etc. The argument for separation and study of the different parts is simply that the practical problem of over-all drawing limits, based on their interaction, ought then to become better understood.

Forming limits under largely radial-drawing conditions are by far the best understood. Because of the basic non-steady state nature of such drawing, the required loads tend to be applied at the weakest link in the system, to material like that near the bottom of a cylindrical-cup wall which has been strengthened the least by any cold work in drawing. Frequently, failure consists of a plane-strain necking down of the side-wall



material.<sup>3</sup> Steps to improve the limit have generally involved: redistributing load away from this section of least load-carrying ability (as by rubber forming, the use of a high-friction punch face, etc.), reducing load by increasing process efficiency, or possibly lowering deformation strength of the flange region with local heating. Generally, little improvement has occurred from changing properties uniformly throughout a sheet. The possible importance of strain hardening characteristics has been considered many times; particular attention has been given to different measures of a material's resistance to necking under tension, such as the uniform tensile elongation, strain-hardening exponent,  $n$ , in the  $\sigma = K\epsilon^n$  approximation of the true stress-strain curve, and the tensile-to-yield strength ratio.<sup>3-12</sup> Yet the drawing limit has remained rather insensitive to variations in these quantities, strikingly so in comparison with the effects to be anticipated on the limit in a steady-state operation such as wire drawing.<sup>12</sup> In the extreme case of the "drawing anomaly", the limiting blank diameter for a cylindrical flat-bottom cup may actually decrease slightly as strain-hardening capacity increases.<sup>3,6,7</sup> However, a relatively simple rationale of such observations can be made which shows that the limit under conditions of radial drawing is, to a good approximation, a measure only of the natural base of logarithms; material properties tend to drop out of the argument.<sup>12</sup>

An important possibility for metallurgical control over the radial-drawing limit has recently been established by Whiteley<sup>11</sup> who demonstrated that with a plastic anisotropy giving increased "thinning resistance", material in the potential failure region is strengthened relative to that



in the deforming flange. The anisotropy is described by a coefficient,  $R$ , measured in tension testing, which is the ratio of plastic strains along width and thickness directions; it tends to be constant in a given test, being 1 for isotropic material and  $>1$  for the material of improved drawability. When conditions permit, it is convenient to regard  $R$  as uniform and independent of direction in the plane of the sheet, or to consider the sheet to have planar isotropy.

Understanding of limit control in the area of punch stretching is not so well developed. There are various indications that properties contributing to this limit are not necessarily significant in radial-drawing. One is the increasingly widespread use of the Swift Cup Test for drawability based on limiting-blank measurements with both flat-bottom and hemispherical (stretch inducing) punches.<sup>13</sup> Another is the establishment of stamping-severity classifications in which stretching plays a key role.<sup>14</sup> It is evident from many experiments that increased strain-hardening capacity contributes to deeper parts when the design, as in the case of a hemispherical profile, leads to extensive punch stretching.<sup>3,6,7,15</sup> In important early work by Lankford, Snyder, and Bauscher<sup>16</sup> a particular complex asymmetric stamping was produced with most success from sheets satisfying a required minimum value of the parameter ( $R \times n$ ), which emphasizes the possibility of interaction between the two kinds of limits. Friction in the punch-sheet interface is also recognized as influencing the punch-stretching limit; work on the drawing of round-bottom cups has shown that failure can be shifted from a drawing to stretching location and closer to the pole of the cup by improving punch-face lubrication.<sup>6,7,15</sup>

Stretching may be terminated by plastic instability. Therefore the previous related work and particularly the detailed theoretical studies of Hill<sup>17,18</sup> and Swift<sup>19</sup> have some important implications for the problem at hand. In the simplest example of a rod under uniaxial tension, deformation can continue without change in load when

$$\frac{d\sigma}{d\epsilon} = \sigma \quad (1)$$

A more general condition for a sheet loaded uniformly in its plane (plane stress) with a ratio of intermediate,  $\sigma_2$ , to largest,  $\sigma_1$ , principal stresses (the stress ratio) of  $X = \sigma_2/\sigma_1$  is

$$\frac{\bar{d}\sigma}{\bar{d}\epsilon} = \frac{\bar{\sigma}}{Z} \quad (2)$$

where

$$\bar{\sigma} = \sigma_1 (1 - X + X^2)^{1/2} = \sigma, \text{ for pure tension } (X = 0) \quad (3)$$

$$\bar{\epsilon} = \epsilon_1 \frac{2(1 - X + X^2)^{1/2}}{2 - X} = \epsilon_1, \text{ for pure tension } (X = 0) \quad (4)$$

and  $Z$  is a function of the stress ratio,  $X$ . The graphical solution of equation 2 is illustrated in Fig. 1 for different values of  $Z$ .

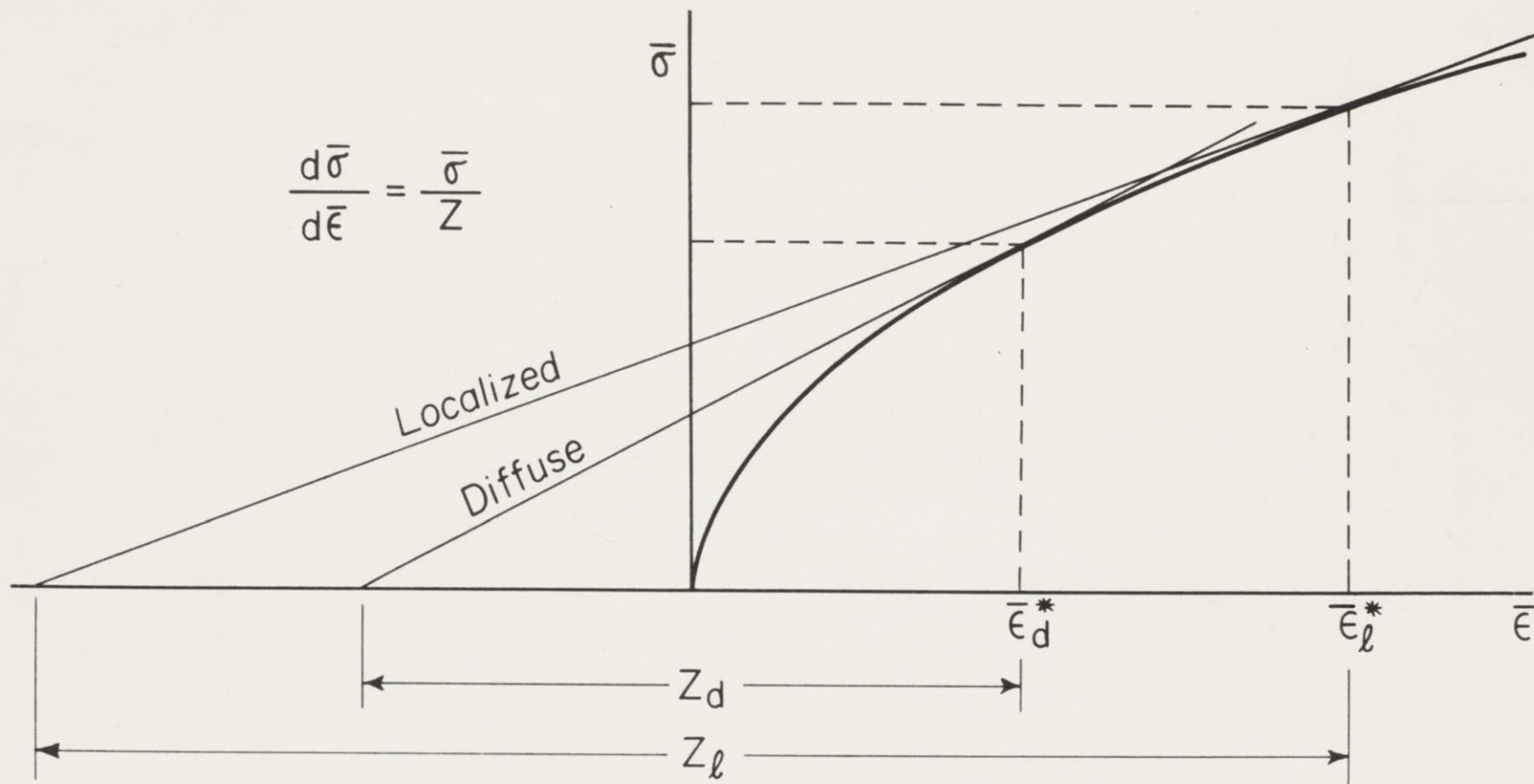


Fig. 1 - Graphical Determination of Instability Strain in a Sheet Uniformly Loaded in Its Plane.  $Z$  is a function of the principal stress ratio  $\sigma_2/\sigma_1$  ( $\sigma_3 = 0$ );  $Z_d$  relates to the beginning of diffuse and  $Z_l$  to the beginning of localized necking. For uniaxial tension,  $\bar{\sigma} = \sigma$ ,  $\bar{\epsilon} = \epsilon_1$ ,  $Z_d = 1$ , and  $Z_l = 2$ .



Two modes of unstable flow are indicated in Fig. 1. The first is broadly and symmetrically distributed about the loading directions and is termed "diffuse necking"; it is encountered at  $\bar{\epsilon}_d^*$  when

$$Z_d = \frac{4(1 - X + X^2)^{3/2}}{(1 + X)(4 - 7X + 4X^2)} \quad (5)$$

The alternate mode, setting in at  $\bar{\epsilon}_l^*$ , involves a thin band of flowing material inclined at an angle  $\alpha$  (Fig. 2) across the sheet to give localized necking. Now

$$Z_l = \frac{2(1 - X + X^2)^{1/2}}{1 + X} \quad (6)$$

A necessary condition for localized necking is that no strain be imposed on the non-deforming material adjacent to the flowing region, or that no extension occur along the trough in the neck (Fig. 2). Thus a local neck might be accommodated as long as  $d\epsilon_2 \leq 0$ . According to the Levy-Mises equations,  $d\epsilon_2/d\epsilon_1 = (2X - 1)/(2 - X)$  for an isotropic ( $R = 1$ ) sheet. Therefore,  $d\epsilon_2 = 0$  is identified with  $X = 1/2$  and  $Z_d = Z_l$ ; the two modes become equivalent and a neck may form at  $90^\circ$  to the  $\sigma_1$  axis. The angle,  $\alpha$ , is determined by the value of  $d\epsilon_2$  relative to  $d\epsilon_1$ , and as long as  $d\epsilon_2 < 0$  ( $X < 1/2$ ),  $\alpha$  is less than  $90^\circ$  and given by

$$\alpha = \arctan \left( \frac{X - 2}{2X - 1} \right)^{1/2}; \quad (7)$$

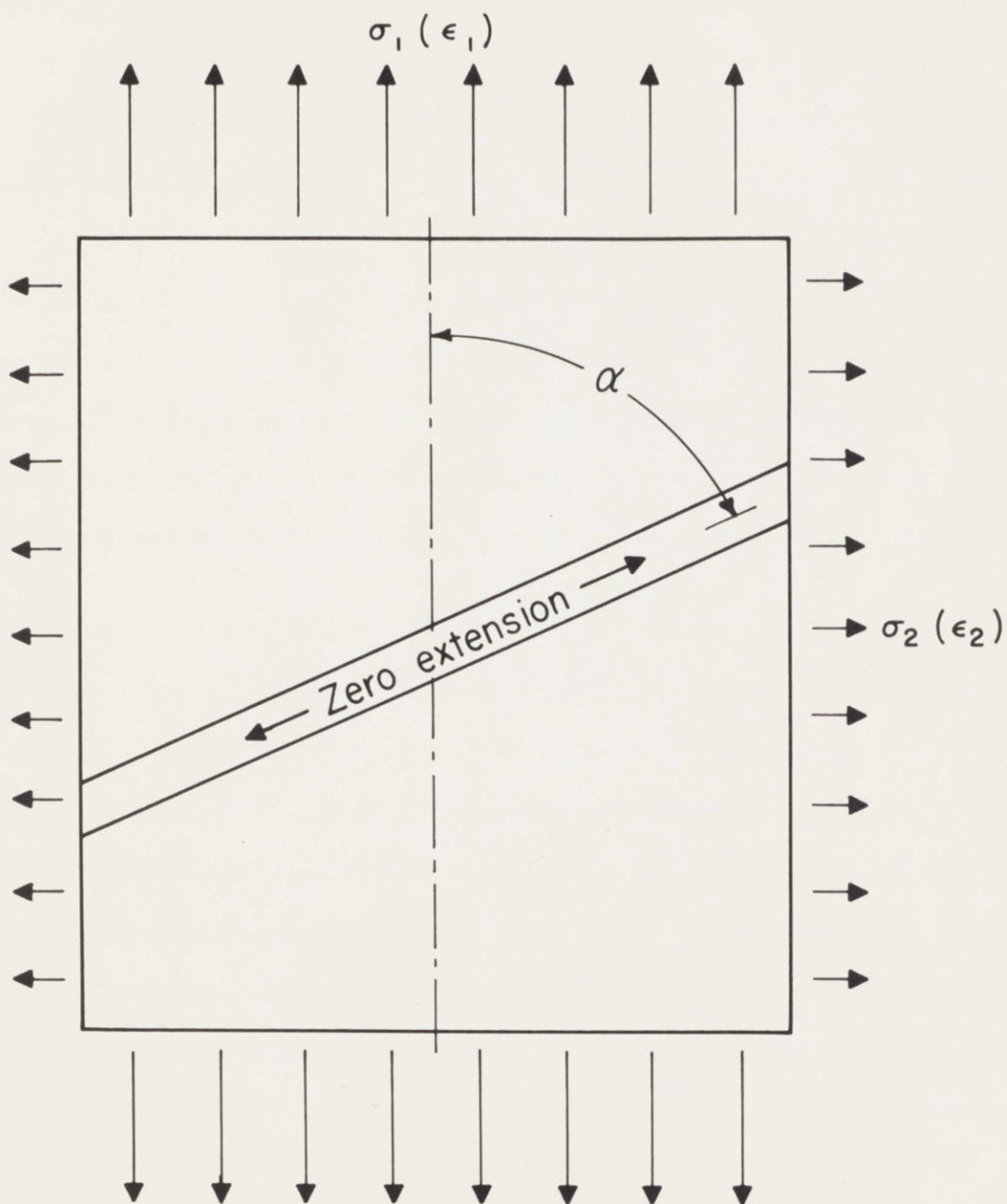


Fig. 2 - A Localized Neck at Angle  $\alpha$ . No extension occurs along the neck. The angle  $\alpha$  is determined by the stress ratio. For uniaxial tension in an isotropic sheet,  $\alpha = 54^\circ 44'$ ; it increases to  $90^\circ$  for  $\sigma_2/\sigma_1 = 1/2$ . ( $d\epsilon_2 = 0$ ).



now the local-necking condition is satisfied at the larger strain, or lower work-hardening rate ( $Z_l > Z_d$ ), because of the further restriction that  $d\epsilon = 0$  along the neck. When  $d\epsilon_2 > 0$  ( $X > 1/2$ ), which would occur everywhere in punch stretching if a sheet were securely clamped, there is no direction of zero extension and localized necking cannot be expected. Conditions for the onset of both diffuse and localized necking in an isotropic material under plane-stress loading are summarized in Fig. 3 with a plot, developed from Hill,<sup>18</sup> of  $\beta = \frac{1}{Z} = \frac{1}{\sigma} \frac{d\bar{\sigma}}{d\bar{\epsilon}}$  vs.  $X$ ; a vertical line in Fig. 3 represents the straining of a material at constant  $X$ , the initial stages being represented at the top of the line or highest  $\beta$ .

If the sheet is characterized by  $R > 1$ , but with planar isotropy,  $d\epsilon_2$  is reduced (algebraically) relative to  $d\epsilon_1$  for a given  $X$ ; the result is that  $d\epsilon_2$  does not become greater than 0, after which localized necking is precluded, until  $X > 1/2$ . The value of  $X$  for this limiting case when  $R$  is changing is shown in Fig. 4. A still more detailed view of the interrelationships between  $\beta$ ,  $R$ ,  $X$ , and the possible necking modes is offered in Fig. 5 where it may be noted that Fig. 3 is a section of Fig. 5 at  $R = 1$ , while Fig. 4 is the projection on the  $X$ - $R$  plane of all curve intersections, of which Fig. 3 gives one example at  $X = 1/2$ . A more detailed development of the subject of plastic instability is contained in Appendix A.

From these various sources some limited background can be obtained for the problem of punch-stretching limits. A number of issues remain unclear, however. The development of unstable flow and eventual fracturing, the influence of material and processing variables and their control,

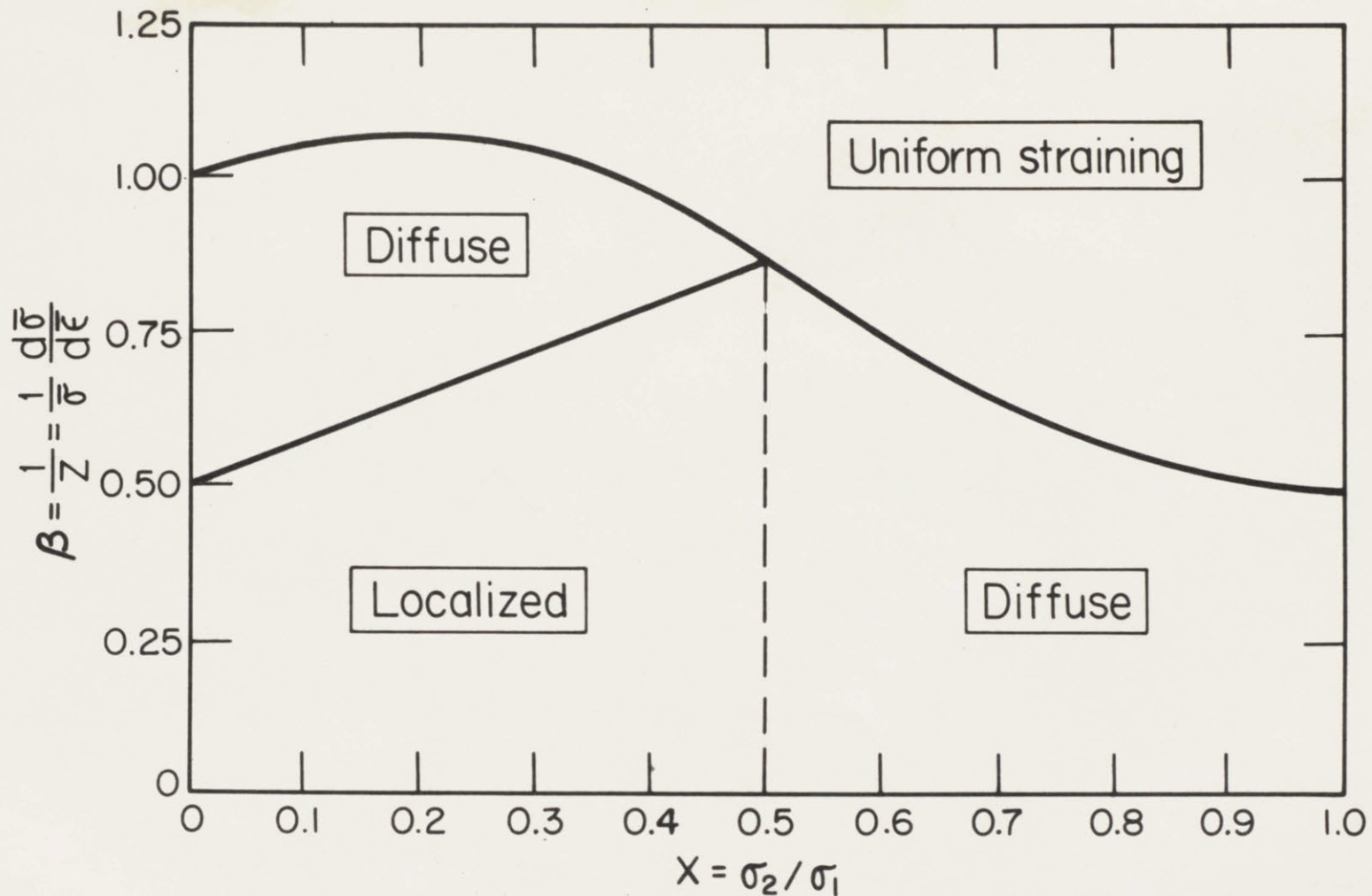


Fig. 3 - The Development of Unstable Flow as Influenced by Stress Ratio,  $X$ , and Strain-hardening Characteristics, Measured in terms of  $\beta$  (Isotropic Sheet). Deformation at constant  $X$  is represented by a vertical line on the abscissa. Deformation begins at high  $\beta$ , a decrease in  $\beta$  indicating increased straining along stress-strain curve. For  $X > 1/2$ , geometrical restrictions prevent localized necking. Development has been based on an analysis of Hill.<sup>18</sup>



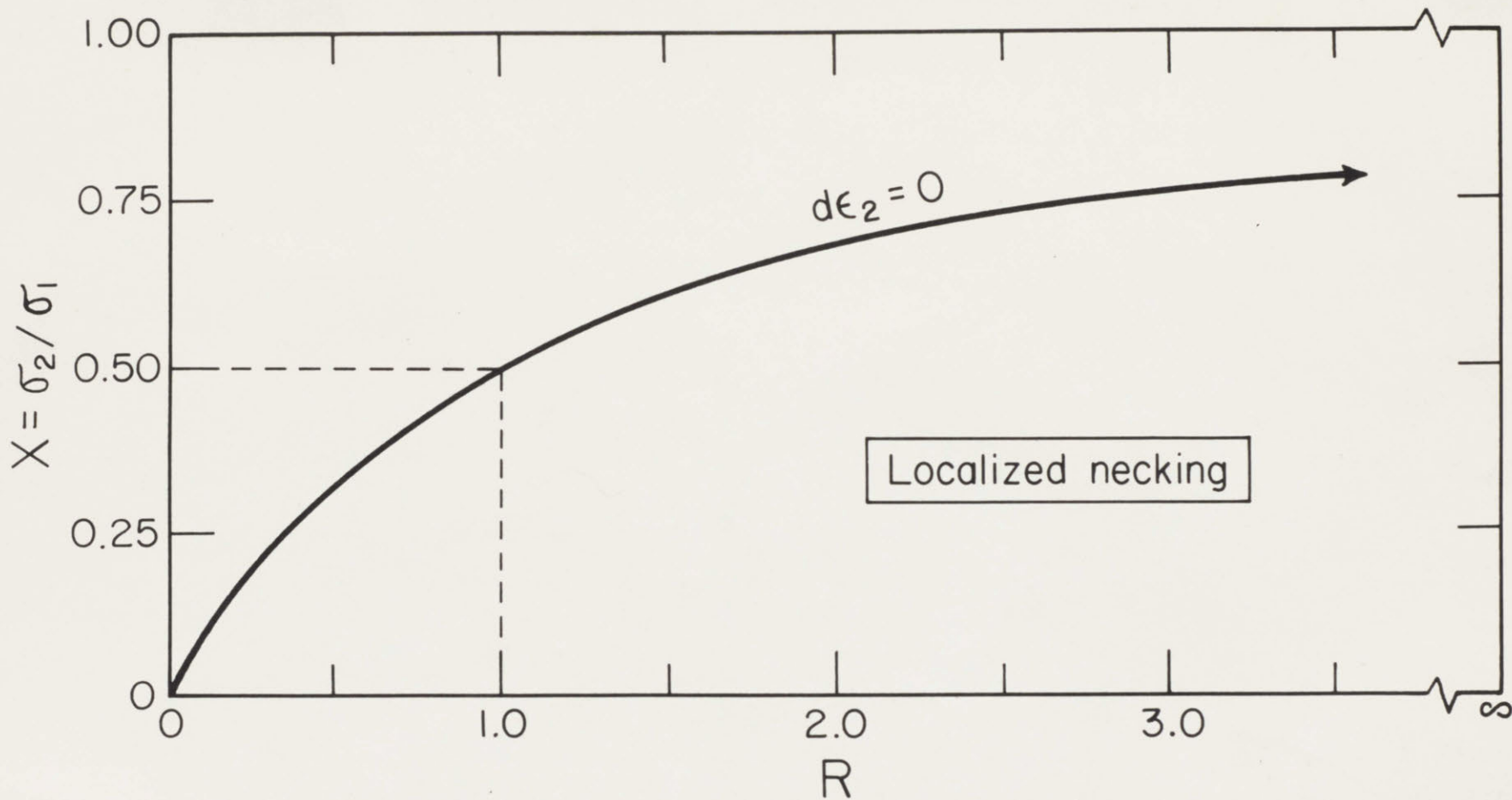


Fig. 4 - Dependence on Plastic Anisotropy of the Limiting (Maximum)  $X$  Above Which Localized Necking Cannot Occur.  $R$  is the ratio of width to thickness strain in a uniaxial tension test, and equals 1 only for complete isotropy. In the plotting,  $R$  has been taken to be independent of direction in the sheet (planar isotropy). Development has been based on an analysis of Hill.<sup>18</sup>

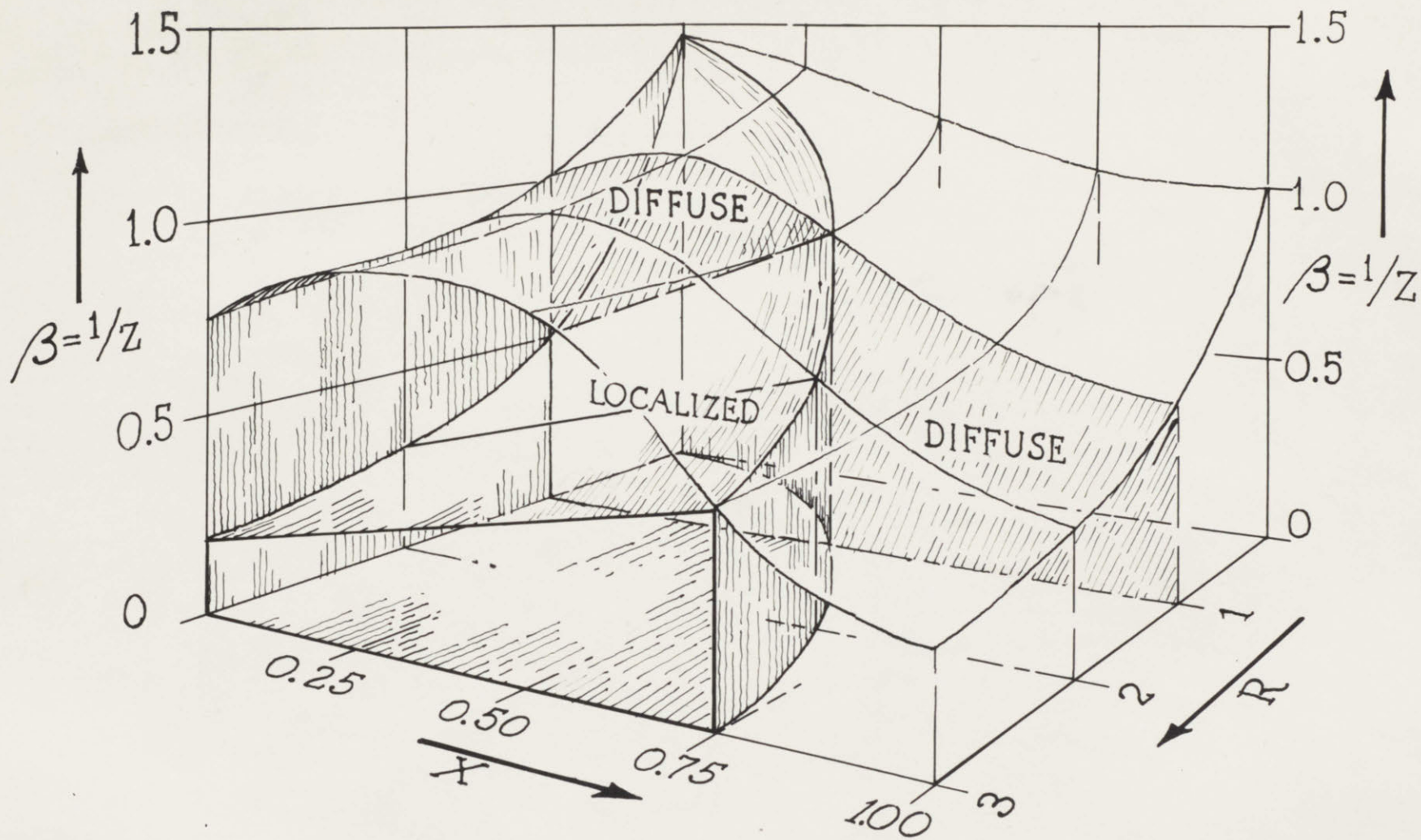


Fig. 5 - A Three Dimensional Representation of How Unstable Flow Develops Under Different Conditions of  $X$ ,  $R$ , and  $\beta$ . A section at  $R = 1$  (isotropic sheet) is given in Fig. 3. Projection of the curve intersection (limit for localized necking) on the  $X$ - $R$  plane is presented in Fig. 4. Development has been based on an analysis of Hill.<sup>18</sup>



still require more thorough understanding; one practical consequence is a substantial gap between available theory and practice. The program reported below was intended to reduce this gap with some systematic experiments under well-defined conditions of punch stretching.

## II. MATERIALS AND PROCEDURES

Materials: Descriptions, properties, and a system for coding seven experimental materials, all in the form of 20-gage sheets, are summarized in Tables I and II. Stress-strain curves,  $\bar{\sigma}$  vs.  $\bar{\epsilon}$  (Eqs. 3 and 4) were established, in part, with specimens taken from the as-received sheets at  $0^\circ$ ,  $45^\circ$ , and  $90^\circ$  to the rolling direction and tested in tension in an Instron machine. To extend the curves beyond necking, strips of 2-inch width,  $0^\circ$  and  $90^\circ$  to the rolling direction, were prestrained by further rolling to various total strains in increments of about  $\bar{\epsilon} = 10\%$  and then tested in tension.<sup>20</sup> The machined gage section in all cases was 6.5-in. by 0.5-in. Periodic strain measurements were made on the as-received specimens with dividers, scale, and micrometer; load-extension curves were obtained from autographic records for prestrained specimens. Final results are presented in Fig. 6, where curves from the as-received and prestrained specimens coincide in the region of overlap.

Values of  $R$ , the ratio of width and thickness strain, were determined from the slopes of the plots relating one to the other; measurements were made on soft, as-received material during uniform elongation and were constant in a given direction. Variations in  $R$  with direction (Table II), which are measures of the departure from planar isotropy, were small for soft brass, copper, and aluminum; identical  $0^\circ$  and  $90^\circ$  stress-strain curves (Fig. 6) are likewise indicative of planar isotropy in these soft materials. An average, defined as  $\bar{R} = 1/4 (R_{00} + 2R_{450} + R_{900})$ , was about 1.5 for the steel, which is a typical value for this particular processing



TABLE I  
MATERIALS TESTED

Material	Condition	Code	Yield Strength, psi. (0.2% offset)	Tensile Strength psi.	T.S. Y.S.	Total Elongation % in 2 in.	Uniform Tensile Elongation, %	Rockwell Hardness
1100 Aluminum	Soft	Al (s)	6,210	13,100	2.11	32	25	15T-18
1100 Aluminum	Half-hard	Al (1/2 h)	17,900	19,000	1.06	7	3	15T-53
70/30 Brass	Soft	Brass (s)	19,100	50,400	2.64	57	49	B-28 <sup>+</sup>
70/30 Brass	Extra Hard	Brass (h)	87,000	98,700	1.14	4	1	B-91 <sup>+</sup>
Tough Pitch Copper	Soft	Cu (s)	11,500	33,000	2.87	41	36	15T-56
Tough Pitch Copper	Extra hard	Cu (h)	50,700	56,400	1.11	5	1	B-57 <sup>+</sup>
Al-Killed Steel	Cold Rolled, Annealed	Steel	28,200	46,000	1.63	35	25	B-40 <sup>+</sup>

<sup>+</sup> Converted from superficial hardness measurements.

TABLE II  
PLASTIC ANISOTROPY COEFFICIENTS

<u>Material</u>	<u>R<sub>00</sub></u>	<u>R<sub>450</sub></u>	<u>R<sub>900</sub></u>	<u><math>\bar{R}</math> +</u>
Al (s)	0.78	0.75	0.96	0.81
Brass (s)	0.84	0.80	0.85	0.82
Cu (s)	0.92	0.90	1.00	0.93
Steel	1.43	1.20	2.50	1.56

$$+ \bar{R} = 1/4 (R_{00} + 2R_{450} + R_{900})$$

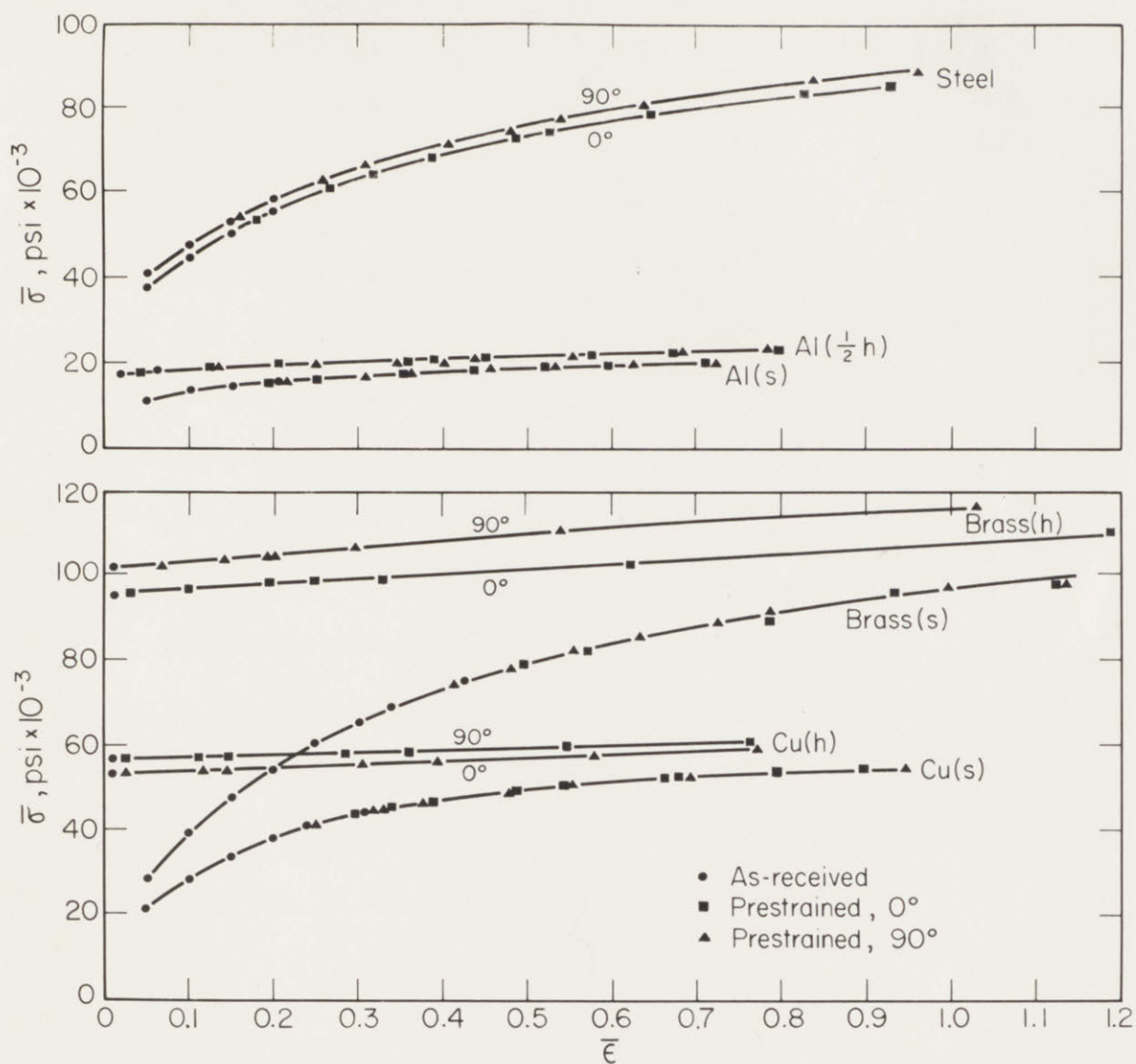


Fig. 6 - True Stress vs. True Strain Curves, 0° and 90° to Sheet-rolling Direction, Obtained by Tension Testing of Both As-received Material and Specimens Prestrained by Rolling. The curves coincide in regions of overlap.



history;<sup>11</sup> the larger value indicates the greater "thinning resistance" so important for increased drawing limits. In the other soft materials,  $R$  being nearly 1 shows them to have been essentially isotropic with respect to strain hardening.

The tangent construction of Fig. 1 was applied to each  $\bar{\sigma} - \bar{\epsilon}$  curve of Fig. 6 and  $\bar{\epsilon}_d^*$  determined for the range of  $X$  from 1/2 to 1, with results presented in Fig. 7; differences could not be found in the  $\bar{\epsilon}_d^*$  values for the  $0^\circ$  and  $90^\circ$  directions. In calculating values of the subtangent,  $Z_d$ , materials were assumed to be isotropic ( $R = 1$ ), which was not a very good approximation for steel, although  $Z_d$  is shown in Fig. 5 to be about constant for  $\bar{R} > 1$  from  $X$  of 1/2 to 3/4. The value of  $R$  was not important for hard brass and copper because  $\bar{\epsilon}_d^* \approx 0$ . The component  $\epsilon_1^*$  of  $\bar{\epsilon}_d^*$  for the onset of diffuse necking was also computed from Fig. 7 and Eq. 4 and is plotted as a function of the stress ratio in Fig. 7.

Specimens: Sheets were assembled in stacks, mounted in a lathe and turned to 8-in. diameter discs. After proper cleaning, a polar grid of 20 concentric circles intersecting an inch of radius was printed on each specimen by an essentially standard photographic process.<sup>21-23</sup>

Stretching: The actual punch stretching was confined within a 4-inch circle around the center of each disc. Testing was done at a speed of about 0.1 in./min. in a subpress, illustrated schematically in Fig. 8, that was mounted in a hydraulic testing machine with provision for autographic recording of punch load. Basically the apparatus consisted of a 4-inch

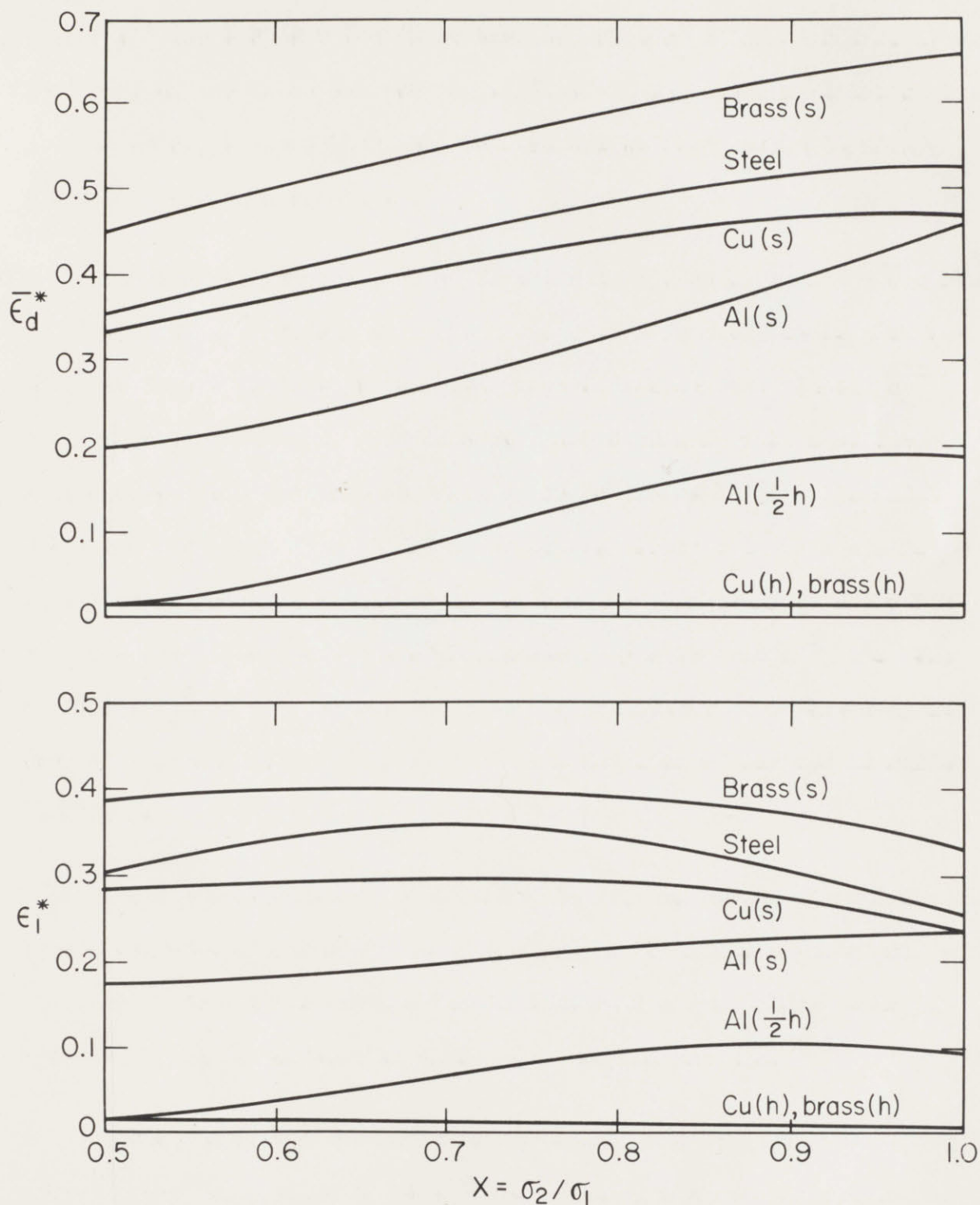


Fig. 7 - Dependence On Stress Ratio of Total Effective Strain,  $\bar{\epsilon}_d^*$ , and Algebraically Largest Component,  $\epsilon_1^*$ , for Diffuse Necking. Computed for All Test Materials by Method of Fig. 1 From Stress-strain Curves in Fig. 6. All Materials Assumed to be Isotropic for the Computation.

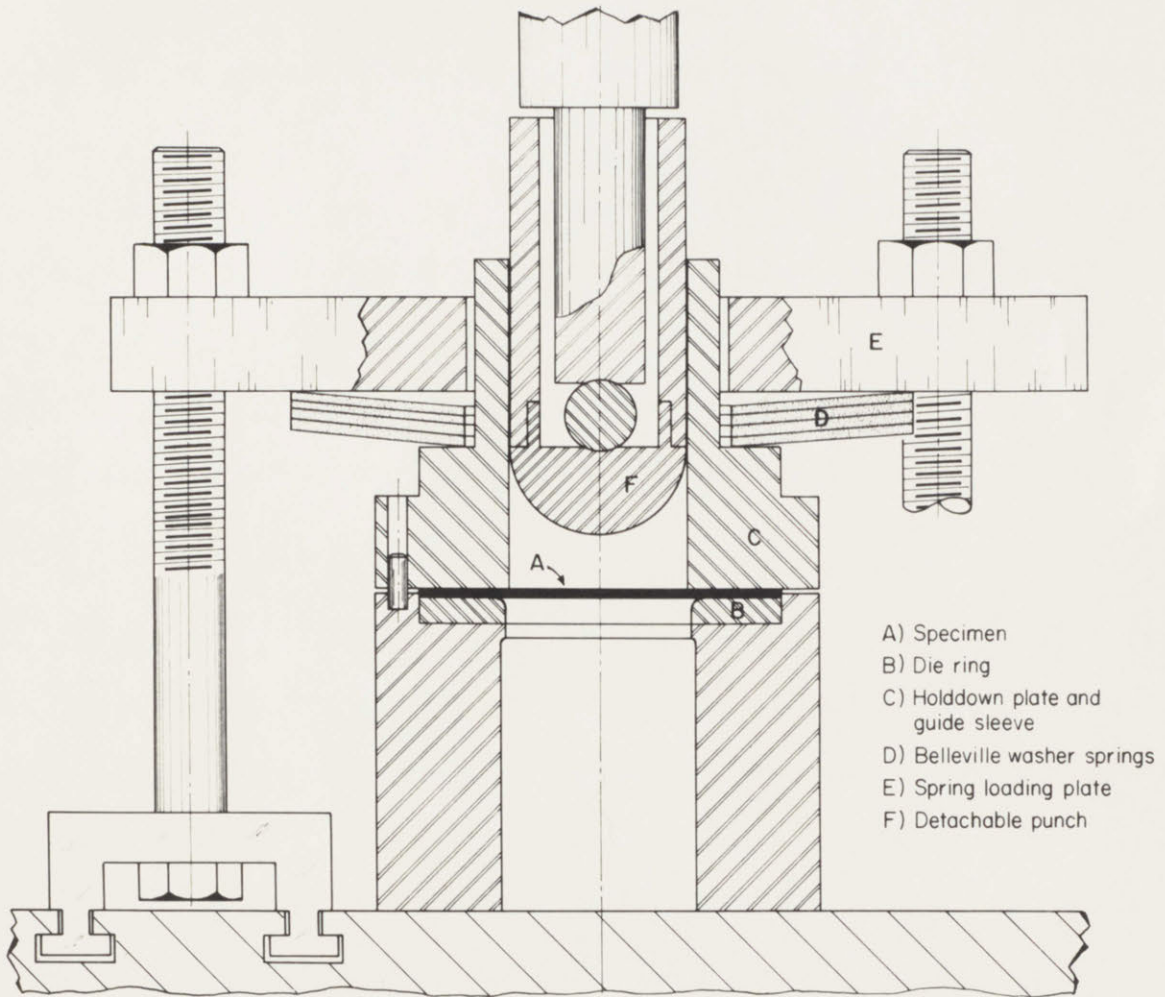


Fig. 8 - Schematic of Subpress.



diameter ram, to which punches were affixed, guided within a sleeve so as to move concentrically through a 4-inch diameter hole in the die plate having an edge radius of 3/8-inch. A blank-holding force of 33,000 pounds, sufficient to prevent drawing-in of the specimen, was obtained by compressing a stack of Belleville-washer springs and maintaining the compression under a plate secured with three large bolts. To insure further against slipping, the outer portions of the blanks located under the clamping ring were roughened by grinding. In all but one experiment, clamping was tight enough that  $de_2 > 0$  over the entire stretching area. Stretching was most often done in increments, the stretched blank being removed for measurements following each interruption.

Lubrication: After screening experiments with several lubricants, two rather extreme conditions of friction were selected. One, without lubricant, was obtained simply by washing all surfaces with soap and water followed by acetone. The other involved a teflon film prepared by brushing an aqueous dispersion over the precleaned specimen and allowing it to air dry; friction coefficient can be estimated to be about 0.01.<sup>24</sup> Cleaning and relubrication were carried out after each increment of stretching. Lubrication codes are teflon (T), and no lubricant (D).

Punch Form: Three designs were used. One was completely hemispherical of two-inch radius, another was hemispherical with only a 1-inch radius joined to the 4-inch ram by a conical surface, and the third was elliptical with 4-inch major and 2-inch minor axes; code designations are H, C, and E respectively.

Strain Measurements: At this point it is convenient to introduce subscripts r (radial) and c (circumferential) as alternatives to the "1" and "2", respectively, that have identified the algebraically largest and intermediate principal strains. Less emphasis is placed on absolute values of stress and these can remain as  $\sigma_1$  and  $\sigma_2$ .

The gridded surfaces were regarded as subdivided into various "elements". With hemispherical punches, each element was taken to lie between two adjacent concentric grid circles, so that there are 40 such circumferential rings between the pole and the clamped rim. For identification, number 1 was bounded by an initial radius  $r_0 = 0.05$  in. and number 40 by  $r_0 = 2.00$  in.; the initial radial dimension between the bounding circles was  $S_0 = 0.05$  in. for all. After stretching, the new dimension  $S$  was measured with a calibrated eyepiece in a hand-held microscope and the radial strain in each element along a longitude line,  $\epsilon_r$ , was computed as

$$\epsilon_r = \ln (S/S_0) = \ln (S/0.05)$$

with an uncertainty of  $\pm 0.015$ . The diameters of all of the enlarged circles were also measured with a mounted and traversing microscope, from which the circumferential strain,  $\epsilon_c$ , along a latitude line, was computed for any element of initial  $r_0 = d_0/2$  as

$$\epsilon_c = \ln (d/d_0)$$



with an uncertainty of  $\pm 0.005$ . The thickness strain was later checked satisfactorily by sectioning and direct measurement with a micrometer.

The polar grid was also used on specimens stretched over the elliptical punch, but an element was identified now as being included by adjacent concentric circles and two neighboring radial (diverging) lines. Measurements were confined to positions along the major and minor axes, these elements being the only ones not undergoing shear distortion. The radial and thickness strains were computed in an identical manner to that used with hemispherical punches. From the spacing  $C$  between the two radial lines bounding an element, again measured with the hand-held microscope, the circumferential strain was computed as

$$\epsilon_c = \ln (C/C_0)$$

with an uncertainty of  $\pm 0.015$ . The dimension  $C_0$  was the chord length between the radial lines at the original element location.

Additional details about these various aspects of Materials and Procedures are given in Appendix B.



## III. RESULTS

Typical distributions of both radial and circumferential strains, from pole towards periphery, are shown at several stages in the stretching of aluminum in Fig. 9. A representative punch-load record is reproduced in Fig. 10.

Cross plotting from such curves as in Fig. 9 gives the strain history of any element at initial radius  $r_0$ . That for the failure-element, located by the vertical arrow, is shown in Fig. 11. Two regions, I and II, could be identified with the radial-strain development. In the beginning, a plastic strain "front" propagated from the pole outwards, and its passage marked the start of straining in an element. With but little additional punch movement, strain now increased at a constant "rate",  $\epsilon_r' = \Delta\epsilon_r / \Delta h$ , with rate being referred to dome height or punch movement. The actual slope of the region-I line proved to be a function of all variables: element location, material, punch shape, and lubrication, but in general it could be related to the steadily increasing surface area.\* The stress ratio associated with an element may be computed from the slopes  $\epsilon_r'$  and

---

\* By a direct graphical method, the distance from pole to rim may be shown to increase essentially in proportion to dome height. The change in this distance is actually obtained from a summation of the radial strain distributed over all deforming elements. Accordingly, the straining rate,  $\epsilon_r'$ , for some element in a pattern might also be expected to be constant.

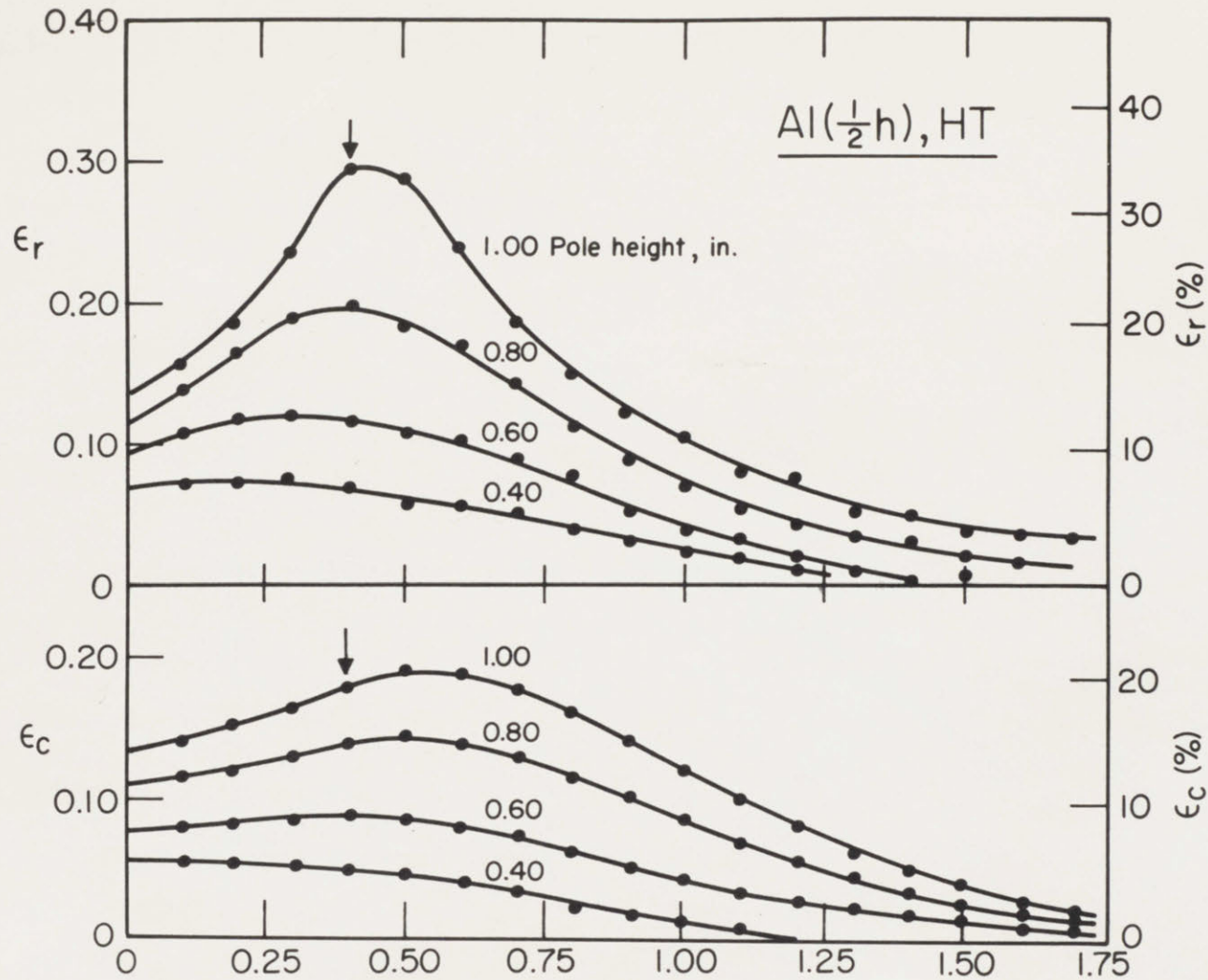


Fig. 9 - Distribution of Radial and Circumferential Strain Across the Dome for Various Pole Heights, Up to Fracture, in Teflon-lubricated, Half-hard Aluminum Stretched over a Hemispherical Punch. Failure location is indicated by vertical arrow. All measurements are plotted at radial positions locating the elements in an unstretched specimen.

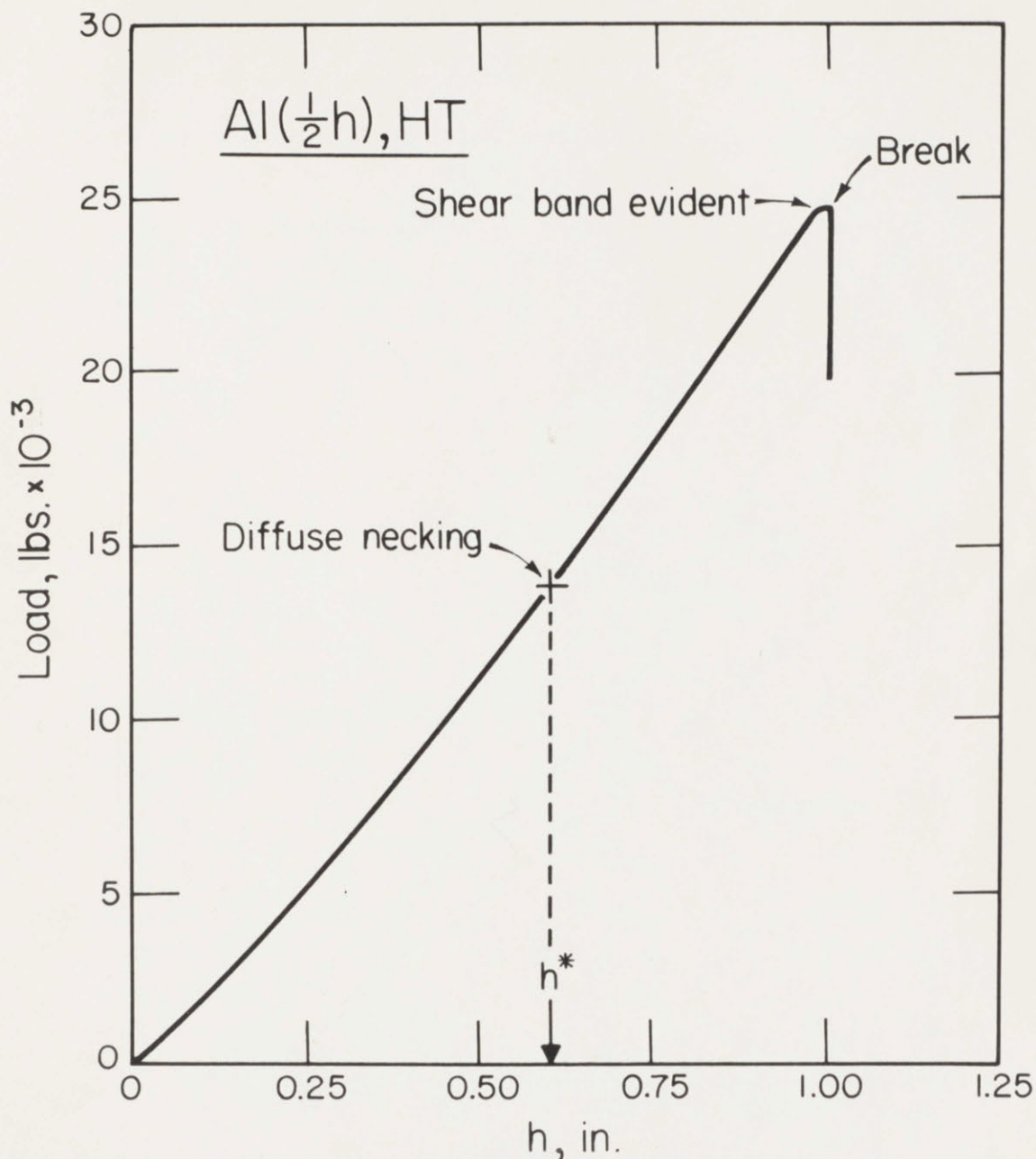


Fig. 10 - Typical Load vs. Pole Height Record for Teflon-lubricated, Half-hard Aluminum Stretched Over a Hemispherical Punch. Note load rising steadily as instability develops. A load arrest occurs with the formation of a shear band.



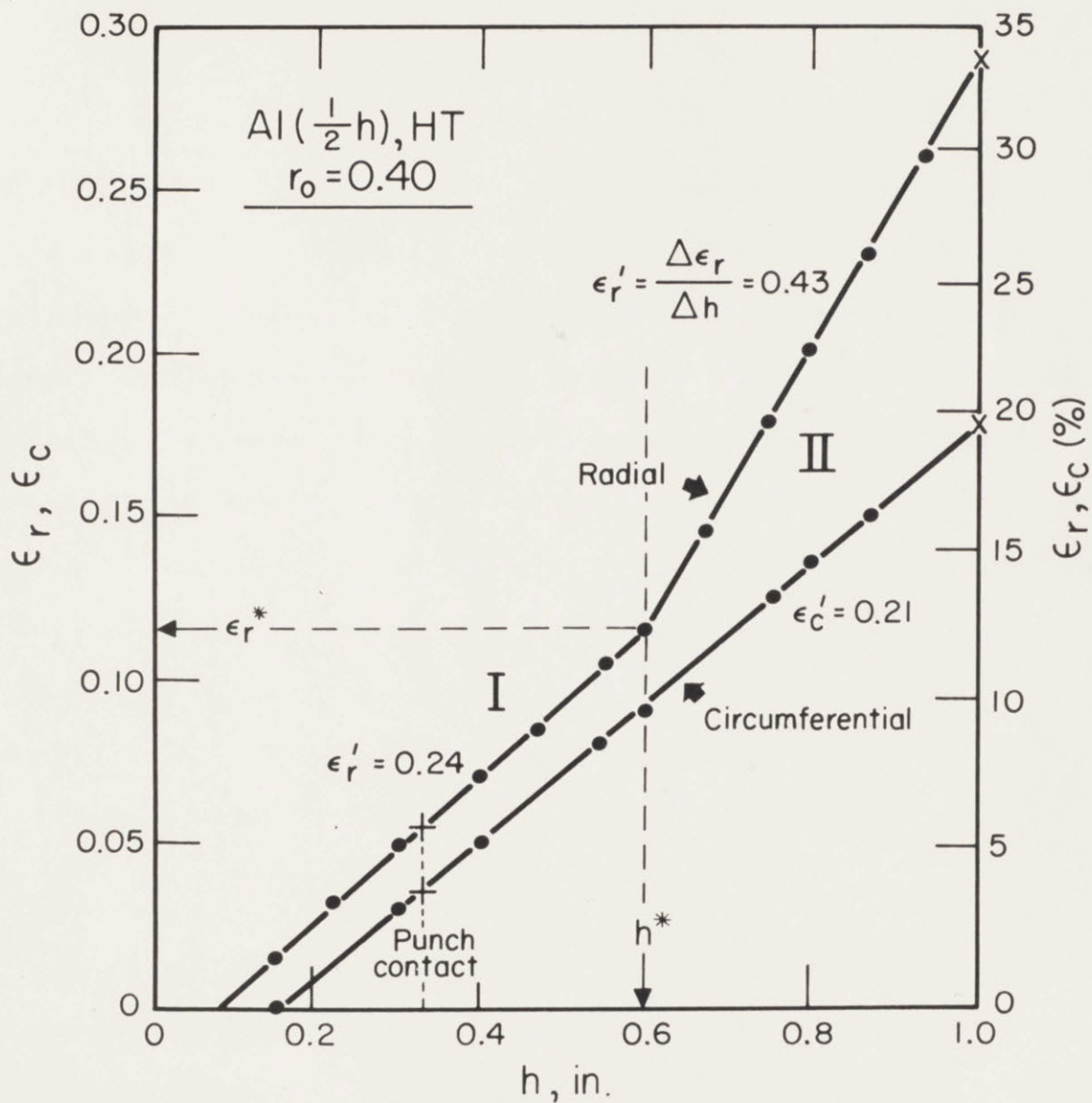


Fig. 11 - Increase of Radial and Circumferential Strain With Pole Height at the Fracture Location in Teflon-lubricated, Half-hard Aluminum Stretched Over a Hemispherical Punch. A discontinuity at  $\epsilon_r^*$  -  $h^*$  separates regions I and II. Fracture is indicated by symbol x.

$\epsilon_c'$  and the Levy-Mises equations (Appendix A),

$$X = \frac{\sigma_2}{\sigma_1} = \frac{\epsilon_r' + 2\epsilon_c'}{2\epsilon_r' + \epsilon_c'} \quad (8)$$

provided that r and c (or 1 and 2) are principal directions. The potential complication in applying Eq. 8 is the shear stress from friction at the interface; this should not have any important effect here, however, even for the unlubricated case, since it is only a fraction (the friction coefficient) of the interface pressure which, in turn, is but a fraction of the sheet stresses. If both  $\epsilon_r$  and  $\epsilon_c$  vs. h plots are straight lines with common origin, then X is constant and the final strains proportional to the strain rates. Interestingly, X was relatively constant throughout a given region except in the case of soft brass (HT) when  $\epsilon_r$  began to develop so much before  $\epsilon_c$  that  $X = 1/2$  during considerable punch movement before acquiring a constant value  $> 1/2$ ; as a result, the ratio of final  $\epsilon_r$  to  $\epsilon_c$  was somewhat greater than that of the rates.

Instability Considerations: A value of  $\bar{\epsilon}^*$  was calculated for each element at the I-II transition. If X was effectively constant, the experimental  $\epsilon_r^*$  and  $\epsilon_c^*$  were used; if it was not, an integration could be made although the departure from constant X was small enough that differences between  $\bar{\epsilon}^*$  obtained in both ways were of little consequence. The  $\bar{\epsilon}^*$  were then compared, with good agreement, to the  $\bar{\epsilon}_d^*$  for diffuse necking under the stress ratios in region I (Fig. 7). When X was constant throughout region I,  $\epsilon_r^*$  was also in agreement with the  $\epsilon_1^*$  component of



$\bar{\epsilon}_d^*$  (Fig. 7). Thus the I-II discontinuity seems well explained by the onset of diffuse necking, which is dependent only upon the stress-strain curve and stress-ratio,  $\lambda$ . The absence of a discontinuity in  $\epsilon_c$  is reasonable on the basis that  $\epsilon_c$  is determined by all radial straining between the pole and element in question. Thus small local changes at the transition would not be likely to appear as a break in the  $\epsilon_c$  trend. A selection of data relating to the strain history of the various elements is presented in Table III. By a statistical test<sup>†</sup> applied to a large quantity of data, including the sample in Table III (see Appendix C), correlation between experimental  $\bar{\epsilon}_d^*$  (and  $\epsilon_r^*$ ) and calculated  $\bar{\epsilon}_d^*$  (and  $\epsilon_l^*$ ) was found to be 0.99.

That element identified by the largest  $\epsilon_r'$  in region I reached instability first and was the origin of the eventual failure. However, in stretching over a rigid tool, the punch load rises even as the unstable flow develops (Fig. 10). The reason is simply that if all flow after onset of instability were to become concentrated in a band around the punch, the polar cap would be lifted away from the punch; but since punch and sheet conform, the adjacent stable material must continue to strain in region I (Fig. 12) and undergo the I-II transition when diffuse-necking conditions are satisfied. The result is a band which spreads out from the place where instability began (Fig. 13) at a rate controlled by punch movement and straining in adjacent stable material.

---

<sup>†</sup> Standard correlation coefficient based on product-moment calculation.<sup>25</sup>



TABLE III  
STRAIN HISTORY OF FAILURE ELEMENTS

Test	$r_o$ , in.	Region I		I-II Discontinuity					Region II		Fracture		
		$\epsilon'_r$	X	$h^*$	$\bar{\epsilon}^*$	$\bar{\epsilon}_d^*$	$\epsilon_r^*$	$\epsilon_l^*$	$\epsilon'_r$	X	$h_f$	$\bar{\epsilon}$	$\epsilon_r$
Al (s)-HT	1.20	0.30	0.83	1.30	0.32	0.34	0.22	0.22	0.65	0.60	1.57	0.59	0.41
Al (s)-HD	1.30	0.30	0.72	1.18	0.29	0.29	0.20	0.20	0.88	0.58	1.30	0.41	0.32
Al (s)-ET <sup>+</sup>	1.60	0.51	0.83	1.04	0.32	0.35	0.23	0.22	0.80	0.73	1.32	0.53	0.36
Al (s)-ET <sup>++</sup>	0.60	0.27	0.78	1.28	0.29	0.31	0.22	0.21	2.00	0.56	1.32	0.48	0.38
Al (1/2 h)-HT	0.40	0.24	0.96	0.60	0.23	0.19	0.11	0.10	0.43	0.79	1.00	0.48	0.30
Al (1/2 h)-HD	0.60	0.21	0.79	0.63	0.17	0.14	0.10	0.09	0.60	0.62	0.82	0.31	0.22
Al (1/2 h)-CT	0.20	0.28	0.98	0.43	0.21	0.19	0.10	0.10	0.58	0.80	0.74	0.49	0.30
Al (1/2 h)-ET <sup>++</sup>	0.25	0.34	0.79	0.42	0.15	0.14	0.11	0.09	0.58	0.68	0.68	0.38	0.30
Brass (s)-HT	1.60	0.23	0.80	None	None	0.60	None	0.39	None	None	2.20	0.51	0.39
Brass (s)-HD	1.65	0.21	0.60	None	None	0.49	None	0.40	None	None	1.65	0.28	0.37
Brass (s)-CT	0.45	0.35	0.85	1.72	0.63	0.62	0.38	0.38	0.44	0.79	1.96	0.77	0.46
Brass (h)-HT	0.30	--	--	0.30	--	0.01	--	0.01	0.27	0.99	0.60	0.15	0.12
Cu (s)-HT	1.20	0.23	0.97	1.64	0.41	0.46	0.25	0.24	1.00	0.63	1.77	0.56	0.38
Cu (s)-ET <sup>+</sup>	1.60	0.41	0.82	1.30	0.41	0.44	0.29	0.29	0.90	0.67	1.47	0.60	0.44
Cu (h)-HT	0.30	--	--	0.30	--	0.01	--	0.01	0.31	0.93	0.85	0.36	0.20
Steel-HT	1.25	0.23	0.82	2.05	0.48	0.49	0.31	0.32	0.55	0.65	2.10	0.57	0.41
Steel-HD	1.70	0.44	0.50	1.83	0.35	0.35	0.31	0.31	--	--	1.84	0.37	0.33
Steel-CT	0.45	0.32	0.99	1.28	0.51	0.52	0.28	0.27	1.30	0.66	1.42	0.74	0.46

+ Major Axis

++ Minor Axis

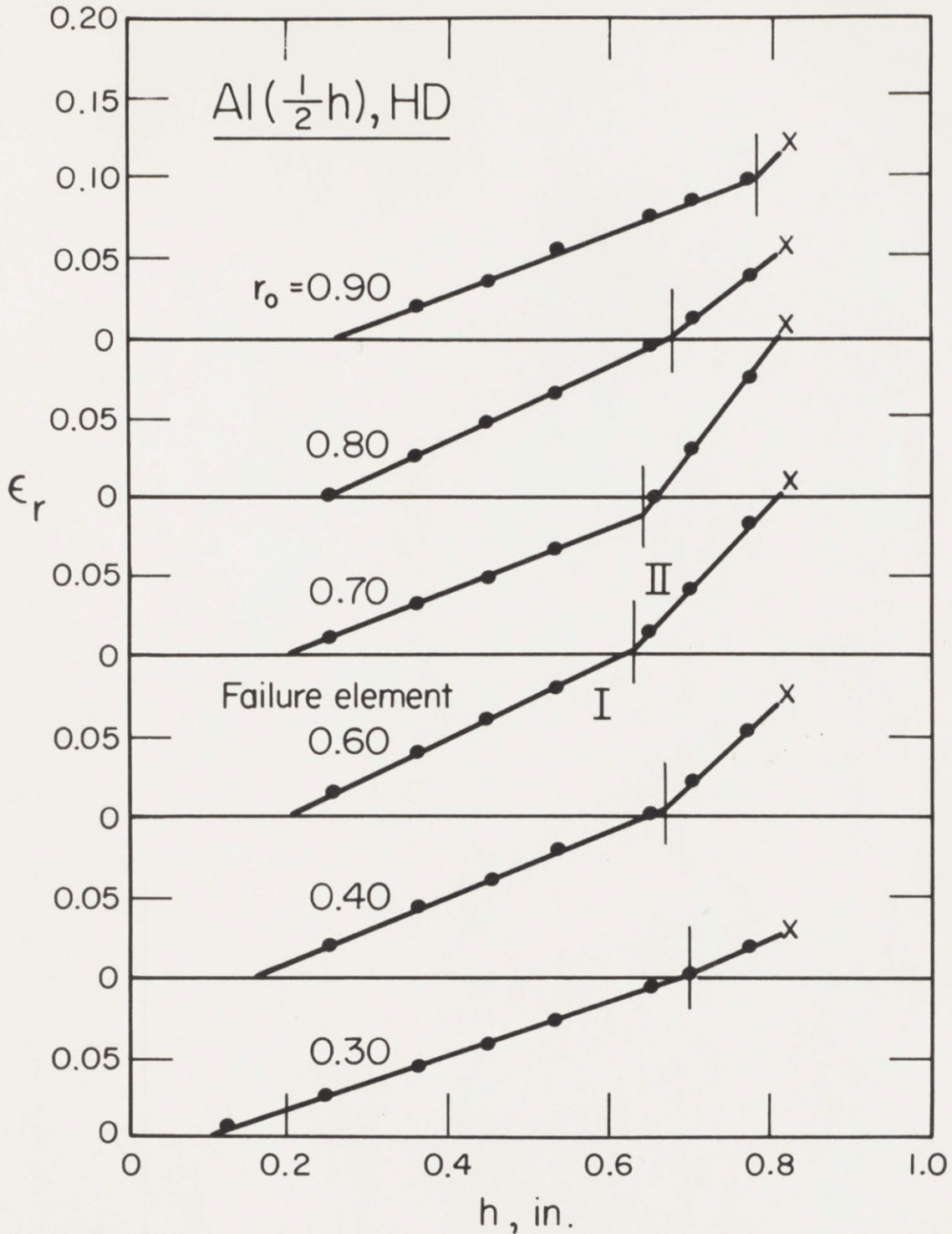


Fig. 12 - Radial Strain vs. Pole Height in Various Elements of Unlubricated, Half-hard Aluminum Stretched Over a Hemispherical Punch. Note strain discontinuity, indicated by vertical line, occurring first at location of eventual failure, and subsequently in surrounding elements. Strain at fracture in the  $r_0 = 0.60$  in. element is indicated by symbol x.

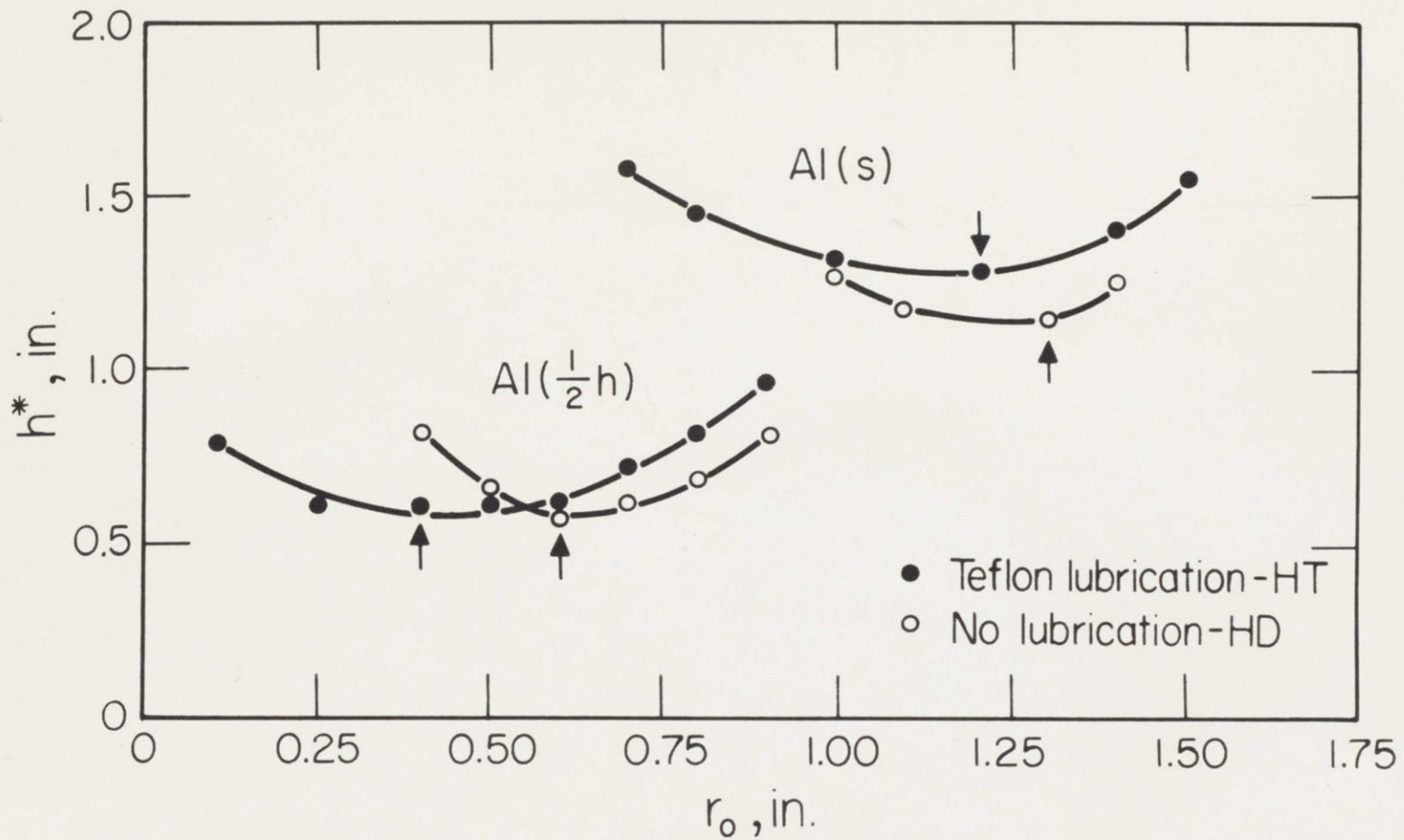


Fig. 13 - Increase in Pole Height,  $h^*$ , as Material Adjacent to the First Unstable Element Satisfies the Diffuse-necking Condition and the Unstable Band Grows Wider. Soft and Half-hard Aluminum, Unlubricated and Teflon-Lubricated, Stretched Over a Hemispherical Punch.



For the somewhat related case of hydraulic bulge testing, again  $d\epsilon_2 > 0$  and localized necking cannot be expected. However, due to the fluid "punch" and straining being most advanced at the pole, instability begins there as diffuse necking with a pressure maximum.<sup>26</sup> Previous measurements<sup>27</sup> of strain at the pole (where  $X = 1$  and  $\epsilon_r = \epsilon_c$ ) may be replotted (Appendix D) as a function of pole height to show reasonably clear straight-line regions I and II with a slope discontinuity at the onset of diffuse necking, as in punch stretching. Apparently considerable flow may also occur under fluid pressure after the instability condition is satisfied and before fracture.<sup>26-28</sup>

Ultimately the stretching limit was reached and a specimen tore at a location that varied rather widely with test conditions. First, however, a trough of local shear became evident on the surface at about the time an arrest appeared in the load record (Fig. 10). Fracture was identified with these events, and the fracture strain was obtained by interrupting at this point for measurements on the failure element at distances away from the incipient tear; in several tests the interruptions came just before the trough formed and measurements then were found to be the same as others made after its appearance. Fracture generally occurred in region II, although in the case of soft brass (HT and HD) it took place in region I before  $\bar{\epsilon} = \bar{\epsilon}_d^*$ . It is noted in Table III that soft brass stretched with lubricant over the fully hemispherical punch (HT) failed at  $\bar{\epsilon} = 0.51$  while  $\bar{\epsilon}_d^* = 0.60$ . (The fact that in this one case  $\epsilon_r = \epsilon_1^*$  is a result of the variable  $X$ , as discussed above.) In a consistent way, failure has also occurred in soft brass in bulge testing before the pressure

maximum and region I-II transition.<sup>28</sup> The depth of punch stretching beyond  $h^*$  is summarized in Fig. 14 where brass is plotted with a negative value obtained by extrapolating the  $\epsilon_r$  vs.  $h$  plot to instability. The trend line is drawn through HT data; others essentially parallel but shifted to the left can be imagined. The latter, as discussed below, are a consequence of more sharply peaked strain distributions around the failure location. Although limiting depths are small (certainly compared to drawing, with depth limits at least twice as great), it is convenient that they are not necessarily fixed just by the onset of unstable flow.

The comparison of radial-strain profiles in Fig. 15 shows that approximately the same maximum level was reached at failure in the four soft materials. However, maximum pole height is proportional to the area under these curves so that the observed stretching limits varied substantially, increasing as strain was more uniformly distributed. In soft aluminum (HT) one-half of the radial strain developed in the "unstable" region II. The profiles of thickness-strain,  $\epsilon_t$ , (Fig. 15) show further that thinning in soft brass was extremely uniform, slight peaks and valleys in  $\epsilon_r$  and  $\epsilon_c$  distributions balancing to give near constant  $\epsilon_t$ ; in aluminum, on the other hand, the high peaks in  $\epsilon_r$  and  $\epsilon_c$  lay at the same locations to give the most nonuniform  $\epsilon_t$ .

Fracturing Considerations: All fracture-strain measurements are organized in Fig. 16 by plotting against the strain-ratio ( $\epsilon_c/\epsilon_r$ ) at fracture. The important detail is the nearly constant value of  $\epsilon_r$  at fracture in the experiments on soft materials. The implication is a critical value of  $\epsilon_r$  as fracture criterion. Since the place of fracturing



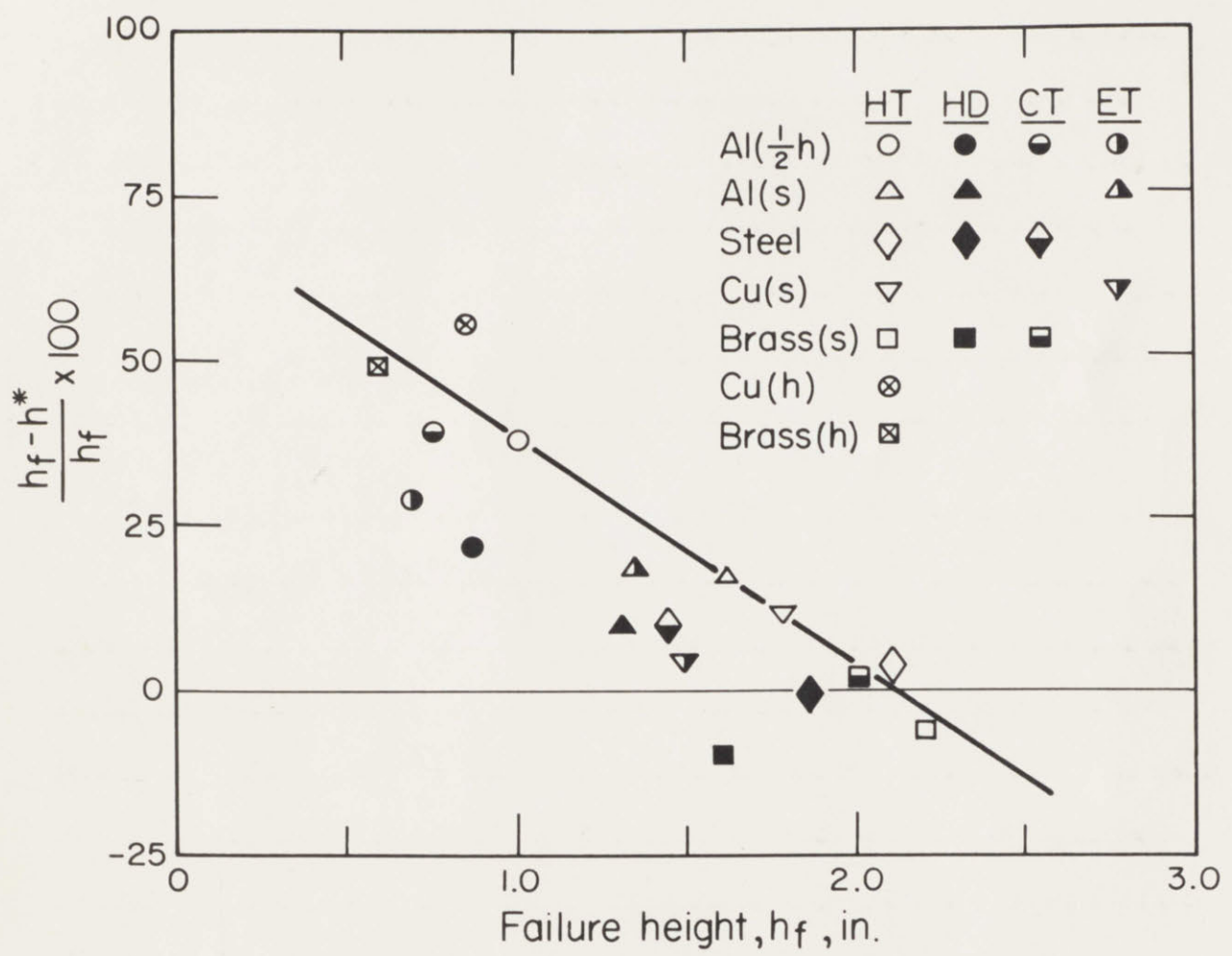


Fig. 14 - Percentage of Pole Height Attained After Instability Related to the Maximum Pole Height at Fracture for All Materials and Test Conditions.



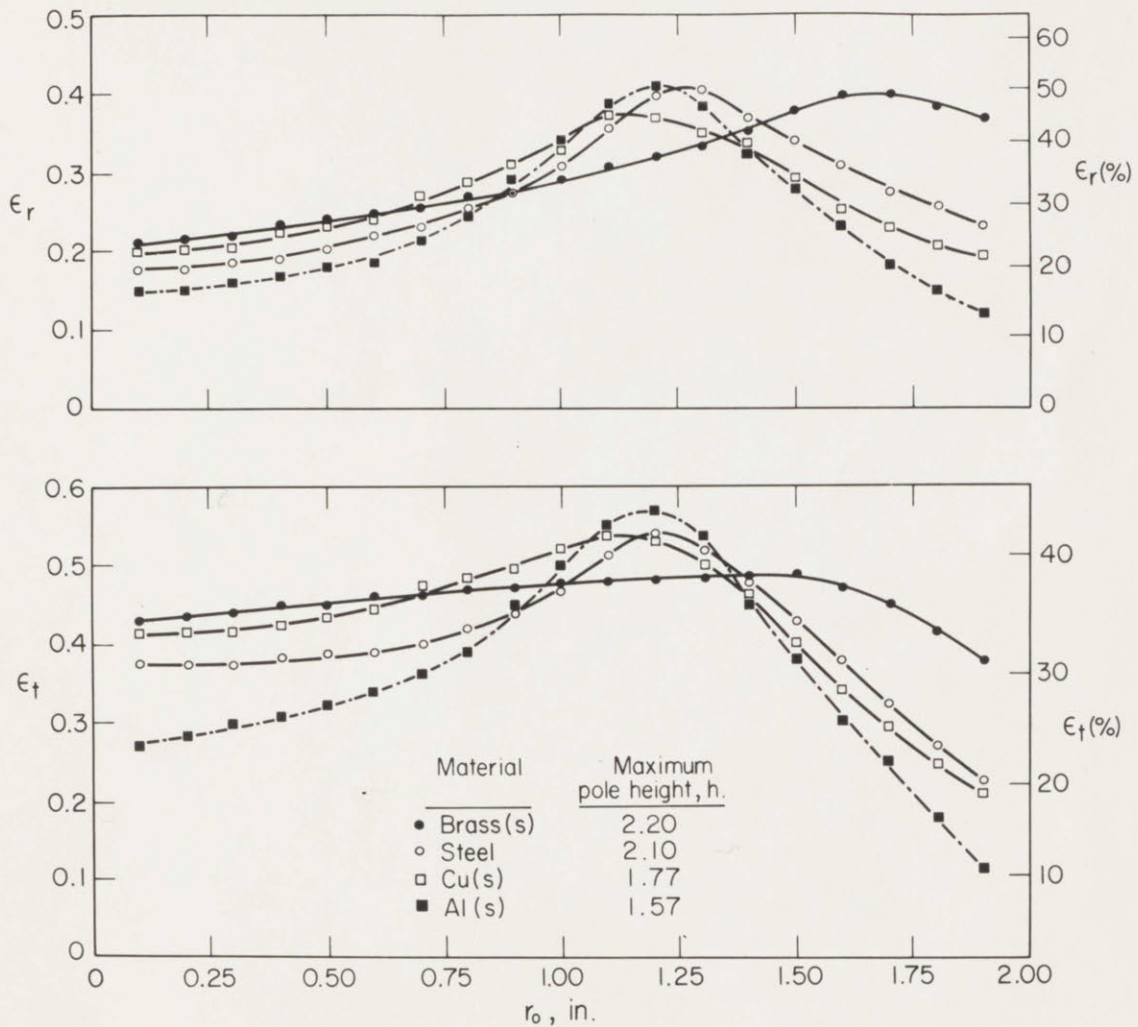


Fig. 15 - Distributions of Radial and Thickness Strain at the Maximum (Fracture) Pole Height for Lubricated, Soft Materials Stretched Over a Hemispherical Punch, Showing Approximately Constant Peak Strain for All Materials. Note uniformity of thickness strain in brass. All measurements are plotted at radial positions locating the elements in an unstretched specimen.

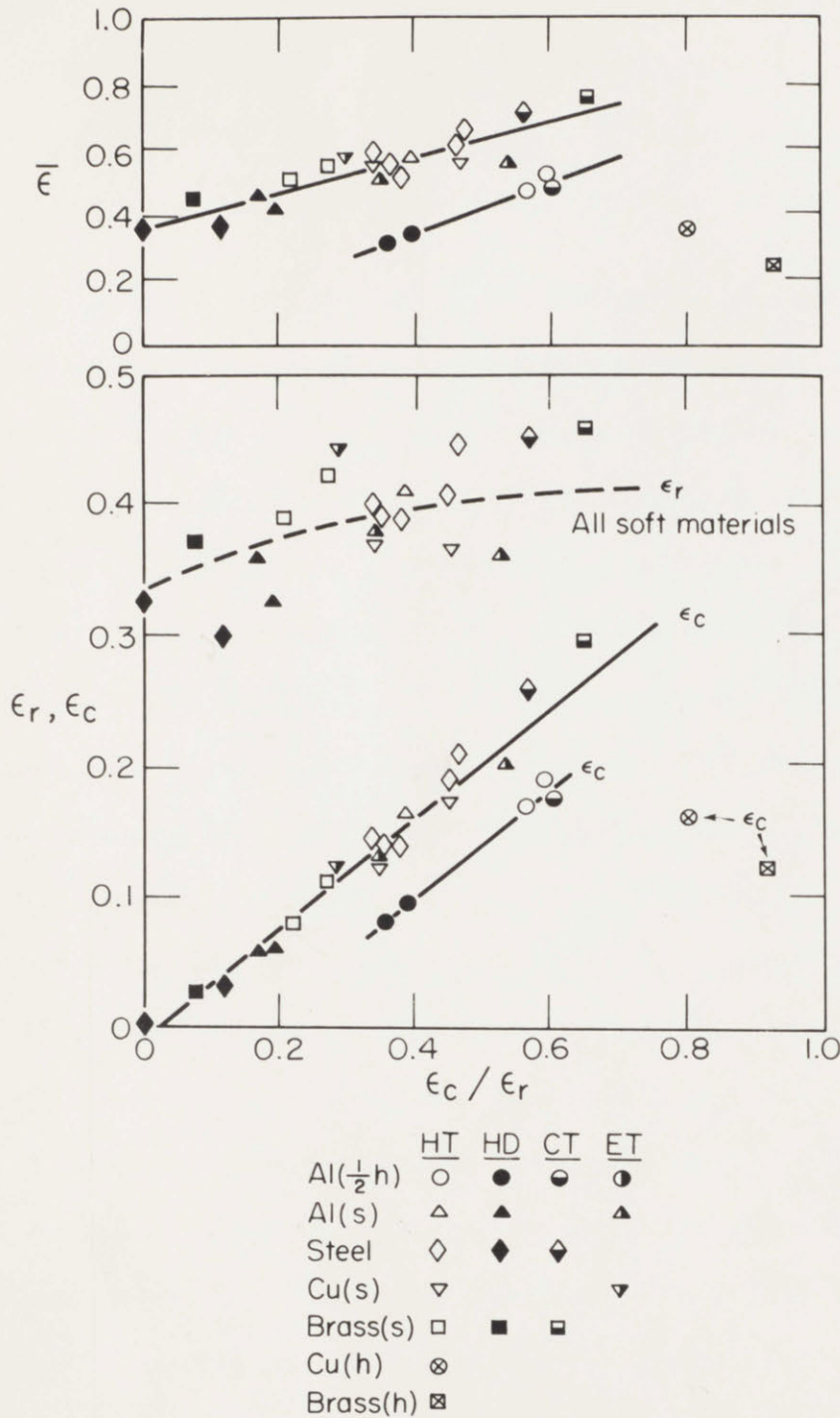


Fig. 16 - A Summary of All Fracture Strain Measurements. The various data are plotted against the ratio of circumferential to radial strain at fracture for all materials and test conditions. The dashed radial-strain line was computed from that drawn through the circumferential-strain points. Note the approximately constant value of radial strain for all soft materials.

changes with experimental conditions, variations shown in  $\epsilon_c$  and  $\bar{\epsilon}$  can be related to fracture location, the trend (in strain) paralleling that in  $X$  which is generally downwards with movement from the pole.

With higher friction, an increased amount of reaction to the stretching load is associated with friction stress at the punch-sheet interface. The strain (and stress) level in material around the pole becomes relatively lower as a result and builds up more slowly towards the place of initial contact between punch and sheet. The fracture location is displaced accordingly and strain distribution becomes increasingly nonuniform (Fig. 17). Since this is the direction of generally decreasing  $X$ ,  $\epsilon_c$  and  $\bar{\epsilon}$  are lower. This effect of friction was illustrated rather directly by removing the lubrication from an aluminum specimen (HT) part way through a test (Fig. 18); the rate of straining over the region of contact immediately became less, while to accommodate the continued stretching the rate of straining was necessarily increased at a greater distance from the pole. Thus the level of  $X$ ,  $\epsilon_c$ , and  $\bar{\epsilon}$  at the fracture site was reduced. In the present work, the failure site without lubrication was never displaced quite as far as to the extreme initial-contact position, although fracture was observed at that location by Loxley and Freeman<sup>7</sup> in stretching unlubricated steel sheets over a 10-inch diameter hemispherical punch.

Material strain-hardening characteristics will also influence the failure site through their direct bearing on the duration of region I straining. If region I is abbreviated, as for aluminum, material near



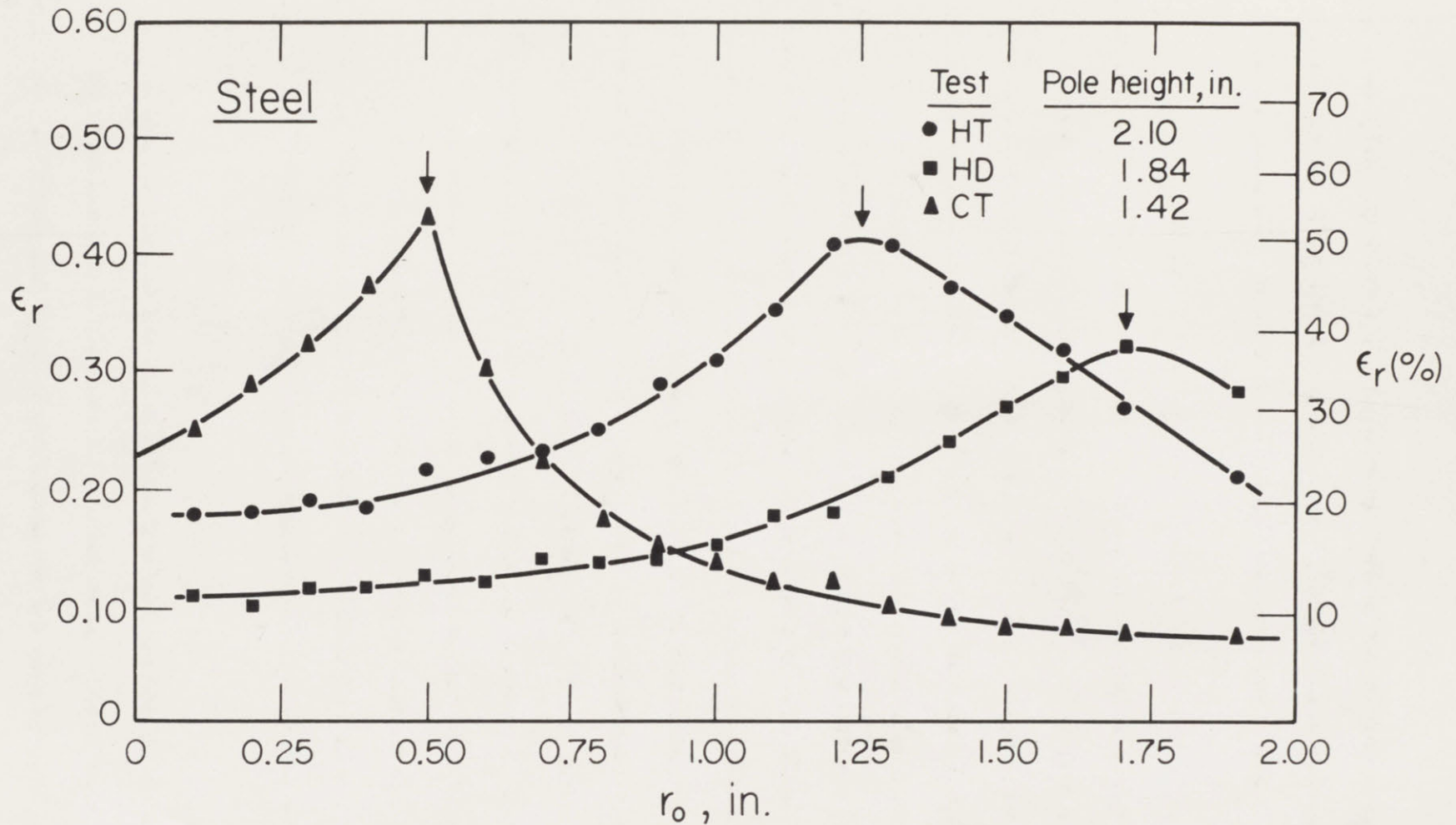


Fig. 17 - Distributions of Radial Strain at Maximum (Fracture) Pole Height in Steel Stretched with Different Lubrication and Punch Geometry. Peak strain for HD taken just prior to localized necking does not represent actual fracture strain. Failure locations are indicated by vertical arrow. All measurements are plotted at radial positions locating the elements in an unstretched specimen.

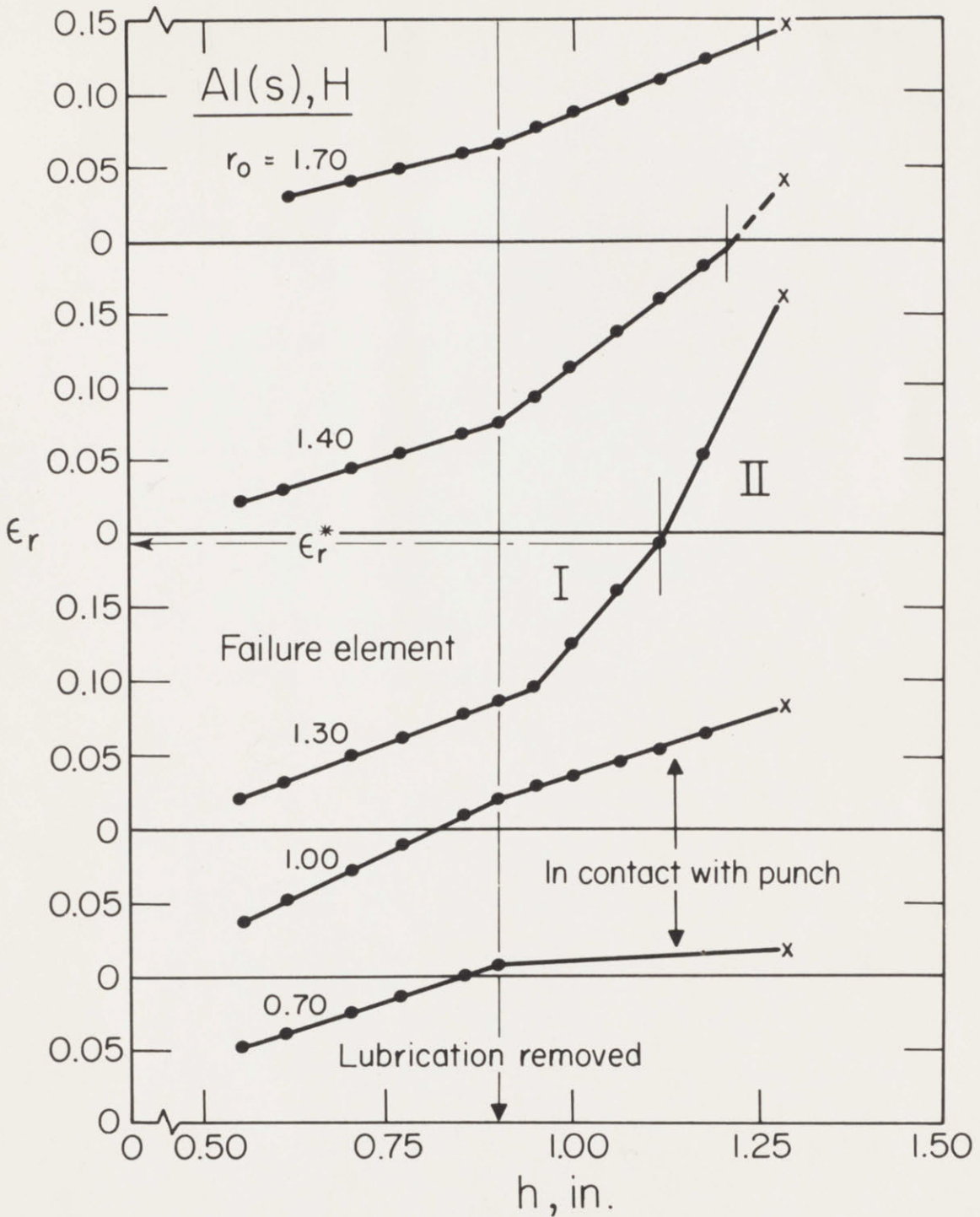


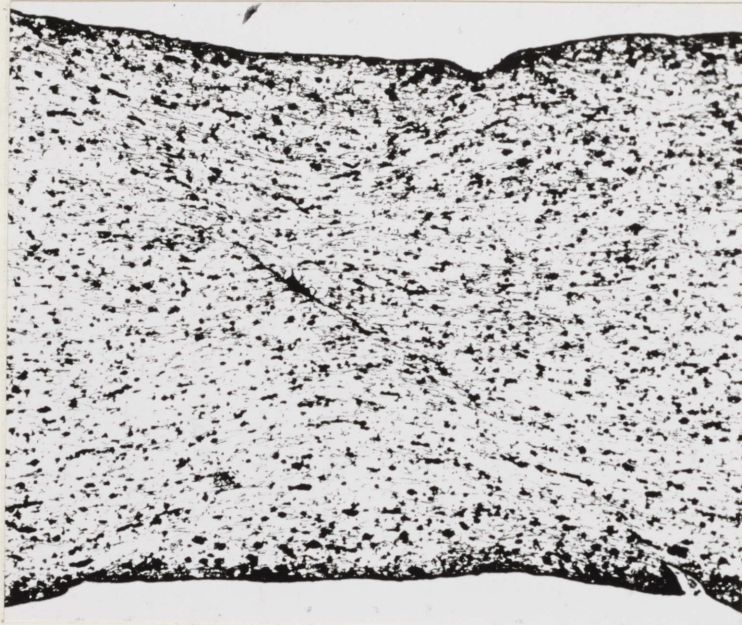
Fig. 18 - Radial Strain vs. Pole Height at Various Radial Locations On Soft Aluminum Stretched Over a Hemispherical Punch. Teflon lubricant was removed during the test. Note reduced straining at locations in contact with punch at time of lubricant removal. Strain at failure height is indicated by symbol x.

the pole quickly passes into stage II so that fracture eventually lies near the pole at generally higher  $X$  and with correspondingly larger  $\epsilon_c$  and  $\bar{\epsilon}$  (Fig. 15).

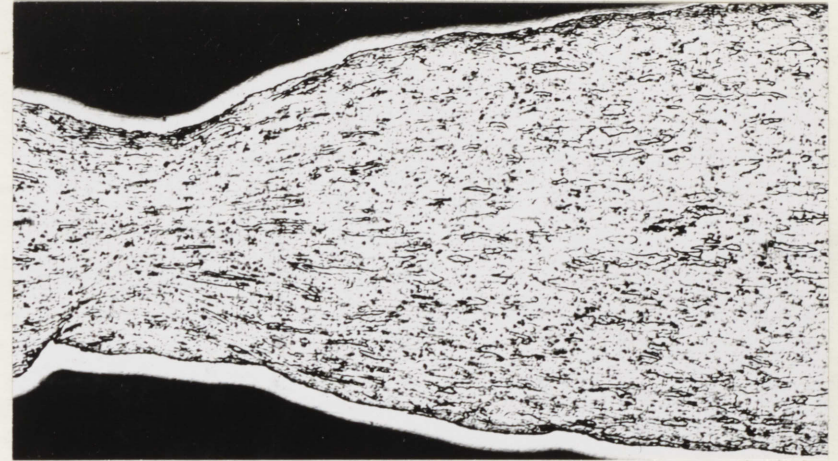
With regard to punch form, a smaller radius (design C in contrast to H) has an effect on strain distribution much more like that of bending under tension; straining tends to be concentrated in the region where the sheet is wrapped over the punch end, which is near the pole and thus locates fracture there (Fig. 17). The observations are similar in stretching over the elliptical punch. Initially, the rate of straining was higher on the smaller-radius minor axis. A hard material with low fracture strain such as the half-hard aluminum soon tore there at little depth. More stretching is possible with soft materials, however, so that the initially high strains could be tolerated; at greater depth the high strain location shifted onto the major axis, near the ends, with the result that soft copper, brass and steel fractured there. A mixture of the two behaviors was found in soft aluminum with the same fracture strain as copper but a much lower instability strain. In this material, fracture took place at an intermediate depth in a continuous path from minor to major axis, as the fracture strain was reached everywhere at about the same time.

The photomicrographs in Fig. 19 were prepared from sections through fracture sites. Intense shear planes, elongated voids suggestive of Roger's<sup>29</sup> void sheets, and cracks being nucleated at the center of the sheet can all be observed. Further detail on fracture examination is given in Appendix E. Certain differences in the profiles of the fracture

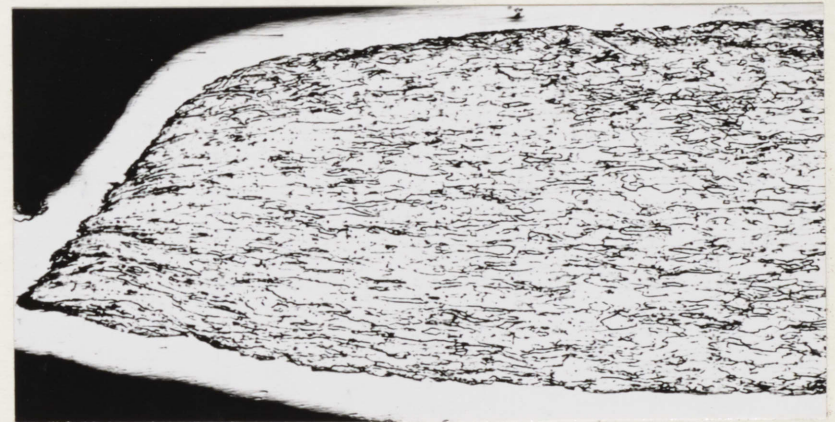




(a) Ammonium Persulfate Etch, X150



(b) Nital Etch, X100



(c) Nital Etch, X100

Fig. 19 - Photomicrographs of Fracture Regions: (a) Hard Copper-HT with Crack Forming at Intersection of Two Shear Planes; (b) Portion of Localized Neck in Steel-HD Showing Crack Forming at Surface; (c) Complete Shear Separation in Steel-HT. All Specimens were nickel-plated prior to examination.

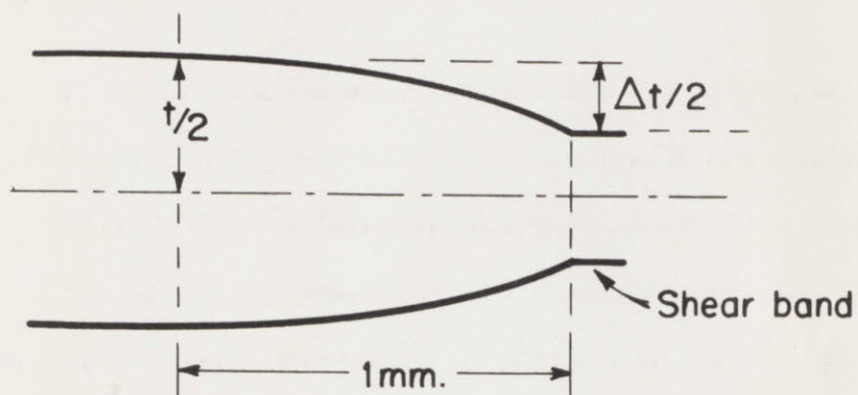


regions shown in Fig. 19 are summarized in Table IV. In only one case could a well-defined localized neck be found similar to that in tension testing: steel HD which, because clamping pressure was too low, underwent some drawing so that at the failure location near the rim  $d\epsilon_c = 0$ .

The various fracturing observations cannot be interpreted in detail without the understanding of ductile fracture that must still be obtained. There is no well-defined criterion, although it has been pointed out that the process is intimately connected with the stress state and microstructure, particularly as affected by processing and deformation history.<sup>30</sup> The beginning in many wrought materials appears to be a formation of pores, due to strain incompatibility, around included particles with different deformation and fracturing characteristics than the ductile matrix. Furthermore, the potential fracture centers tend to be aligned in the usual fiber structure so that the fracture stress and strain are lower in a direction perpendicular to the fiber (or the rolling direction). These circumstances could well explain the lower fracture strain of the hard brass and copper sheets (Fig. 16); fracture centers may have already been enlarged by the preworking. They explain, too, why tearing generally began on a fracture path that was perpendicular to the radial direction and was also parallel (hard materials) or at least tangential (soft materials) to the "weak path" along the rolling direction (Fig. 20).

A constant fracture strain is still another difficult matter to rationalize (Fig. 16). Nevertheless, it has been noted that fracture strain under pure tensile loading is rather similar for a number of ductile metals, even though microstructures may be quite dissimilar as

TABLE IV

SHEET THICKNESS VARIATION AT FRACTURE SITES  
IN TENSION SPECIMENS AND STRETCHED CUPS

Profile reported for distance 1 mm from fracture as  $\Delta t/t$ .

Material	$\Delta t/t$				
	Tension <sup>+</sup>	HT	HD	CT	ET
Brass(h)	0.47	0.15	--	--	--
Brass(s)	0.43	0.26	0.28	0.20	0.13
Cu(h)	0.46	0.22	--	--	--
Cu(s)	0.48	0.20	--	--	0.15
Steel	0.42	0.29	0.41 <sup>+</sup>	0.25	0.25
Al(s)	0.6	0.22	0.26	0.30	0.14
Al(1/2 h)	0.6	0.29	0.27	0.27	0.23

+ Localized Necking



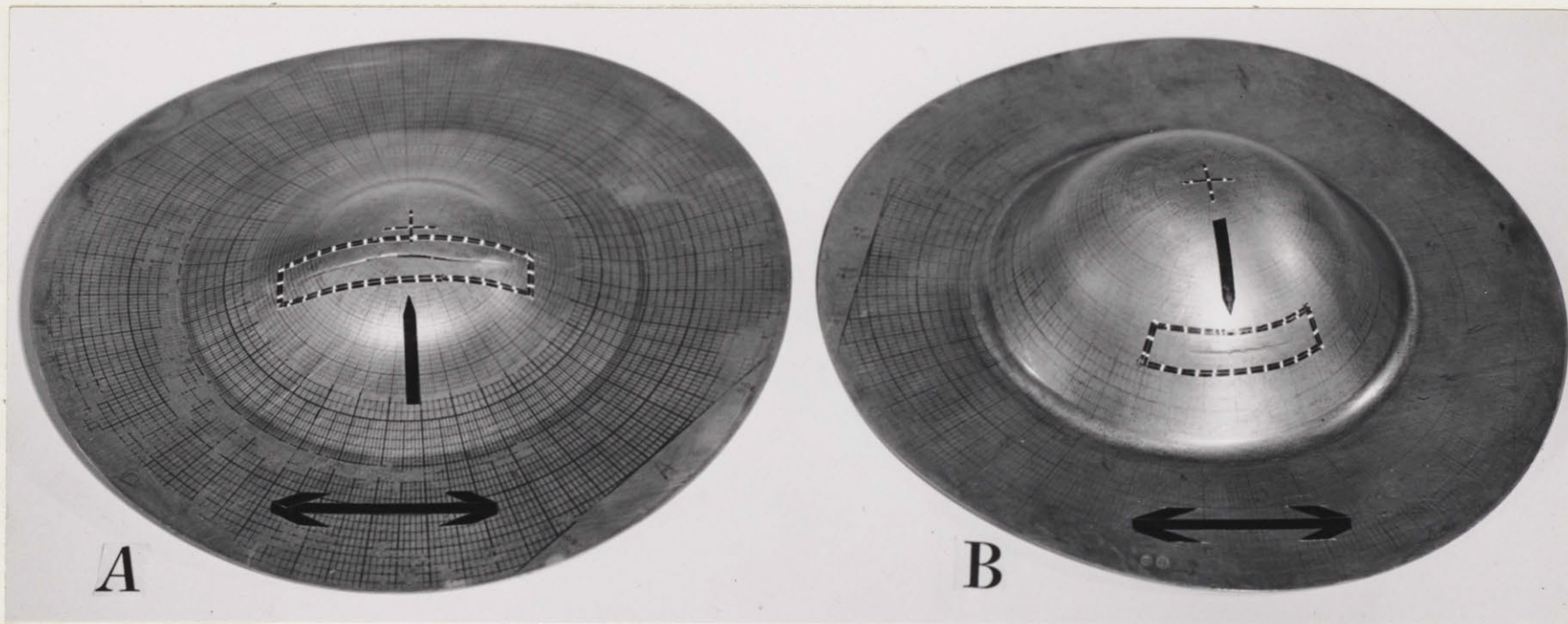


Fig. 20 - Fracture in Hard Brass-HT (Specimen A) and Soft Brass-HD (Specimen B). Rolling direction is indicated by arrow; tear is encircled by dotted line. Fracture began tangential to rolling direction at a location indicated by vertical line. Grid was partially removed by cleaning and handling after testing.

regards extra phases, included particles, etc.<sup>31,32</sup> Apparently, ductile-fracture initiation is influenced by a very fine-scale fiber structure that can be expected whether the microstructure is more or less clean by conventional metallographic appraisal. A higher hydrostatic component in the stress system and especially a higher stress perpendicular to the fiber promote ductile fracturing, which is a further reason for difficulty in relating, directly, fracture in punch stretching and tension testing. The mean principal stress is a measure of the degree of triaxiality, but it can be established in only a comparative way; it would be higher for punch stretching although not known with any certainty.



## IV. DISCUSSION

Limit Control in Punch Stretching: The results have shown that the beginning of unstable flow and subsequent fracturing are determined by stress ratio and material properties. Details of lubrication and punch form basically have little effect. Therefore, from a practical point of view control over the depth of stretching must be based in the first place on control of strain distribution. For greater depth, strain must be distributed more nearly uniformly.

In terms of material characteristics, the requirement is for more persistent strain hardening. Important property trends would be higher  $n$  (if hardening is parabolic,  $\sigma = K\epsilon^n$ ), higher uniform tensile elongation, or higher values of the tensile-to-yield strength ratio. In all cases, strain would tend to be better distributed in the presence of stress gradients. Also, such trends would add to total depth by postponing transition into the more rapid straining and unstable region II, assuming that the transition occurs before fracture. The consequence of impairment to these properties is well known in steel, when ageing depresses their values and forming limits are reduced, especially if stretching is a consideration.<sup>10</sup>

It is evident, too, that lower friction and larger radius of curvature contribute to a flatter strain distribution; for a given peak strain, the distribution is more nearly uniform with greater depth at fracture. The results on soft brass demonstrate the important over-all effects of both sustained hardening and good lubrication in this regard (HT, Fig. 15).



If there is no localized necking, fracture can be expected to terminate the operation and control of fracture strain may also be considered. The opportunity for control would seem to be limited, however, but it does appear that steps to "soften" ought to contribute to higher limiting strain. In this connection, Crussard, Lajeunesse and Pomey<sup>33</sup> have noted that the fracture in elliptical bulge testing lies along the major axis, perpendicular to  $\sigma_1$ . The failure depth is different, however, depending upon whether or not the rolling direction also lies along the major axis; if it does, fracture occurs at lower strain with the effect of less total depth. Thus the anisotropy in fracturing can influence stretching limits.

Still another possibility, although most conjectural of all at this stage, is control based on the plastic anisotropy, conveniently represented by the tensile strain-ratio,  $R$ . It would seem that suppression of local necking in general is worthwhile; therefore, the course to follow if  $X$  is relatively low ( $X \leq 0.5$ ) is to turn to low values of  $R$  ( $< 1$ ), as indicated in Fig. 4. On the other hand, if the operation is characterized by high  $X$ , as in the extreme case of strict punch stretching, the local necking is not a serious problem and preference might be for the highest possible  $R$  (without encouraging a localized neck) since the limiting  $\epsilon_r^*$  does increase with increasing  $R$  as indicated in Fig. 5.

Applications: There should occasionally be practical value in knowing how closely the ultimate forming limit is approached in a particular stamping. Many problems are to be expected if an effort to obtain such information is made at all rigorous, yet some background for this purpose may be extracted from the results of the present experiments.

If depth is the paramount concern, the limit would be determined by either localized necking or fracture; which of these alternatives applies is determined further by the increment of the smaller principal strain in the plane of the sheet,  $d\epsilon_2$ , at a potential failure site. Therefore, strain measurements are in order and would be made preferably with a grid of small circular elements from which both direction and magnitude of principal strains are easily measured. Whether  $d\epsilon_2 > 0$  (fracture) or  $d\epsilon_2 < 0$  (localized necking\*) could be learned from a single, gridded, fully-formed stamping only if stress ratios were reasonably constant throughout the operation. If there was doubt of this, several partial stampings each of different depth would be required for establishing a strain history.

If localized necking is indicated the maximum possible uniform strain can be estimated, for a material with a power-law stress-strain curve, as being within about 15% of the strain-hardening exponent,  $n$ ;<sup>19</sup> for more precision, a graphical construction could be made using a measured stress ratio and the extended stress-strain curve (Fig. 1).

If  $d\epsilon_2 > 0$ , the limiting local strain is that for fracture and can only be known from measurements on the material in question. Such measurements are not now made, but it ought to be possible to obtain them under

---

\* Another limit needs to be recognized here. As a possible extreme,  $d\epsilon_2 = -d\epsilon_1$  when the strain is pure shear, there is no thinning and no instability can occur. The intention now is to consider cases such that  $d\epsilon_2$  does not go below  $-d\epsilon_1/2$ , the condition for uniaxial tension.



useful conditions from hydraulic bulge testing and punch-stretching tests as described here.

At this stage of an analysis, proximity to the limit might be estimated simply by comparing failure strains with the observed maximum strains; if strain vs. depth trends have been established, an extrapolation could also be made to indicate any further allowable depth. The outcome for a successful stamping should be information useful in specifying properties of additional material for the part under study. Still other use could be made of the results in dealing with problems, based on tool design and operation, of controlling lubrication, hold-down pressure, and material flow; the aim of such control would be to create  $d\epsilon_2 > 0$  at the maximum strain area, to minimize peak strains, and to establish flatter strain gradients.

Stamping-severity classifications have been proposed for low carbon steel sheet.<sup>14</sup> More approximate and more easily employed than procedures just described, the basis for evaluation is similar. A material is rated according to Rockwell B hardness, Olsen-cup depth, or the percentage stretch measured on the final part over a one-inch gage length in an initially square grid. Relative to the discussion above, the Olsen and hardness measurements might be viewed as substitutes for the stress-strain curve, with its indication of properties such as  $n$ , and the fracture strain.

Ratings in this system were established for the steel used here simply by measuring the percent radial strain over a one-inch gage length centered on the fracture location. Results were: HT - 41%, CT - 34%, HD - 30%.



Based on 41% stretch in the HT test, as well as  $R_B$  hardness, the sheet would be placed in the highest-severity class, 6K, requiring that it withstand a maximum stretch of 35 to 40% in forming. However, it would not be so rated under CT and HD conditions. In the case of CT, peak strain was actually greater than HT but the steeper gradient brought the average down; the least gradient occurred in HD but now a localized neck terminated straining at the lowest average level. It does appear, therefore, that such ratings are not likely to be conservative. By specifying strain over a one-inch gage length little provision seems to be made either for strain gradients or for localized necking, both of which could lead to failure in a severity-class assigned from measurements when these conditions were absent.

From the viewpoint of the materials producer, certain properties stand out as having particular importance. Stretching limits are extended by high  $n$  (as an example of several related properties) and, if local necking is precluded, by high  $R$ . It is known that drawing limits are improved by higher  $R$ , although relatively insensitive to  $n$ -type properties. From this, a rather old conclusion emerges; for the generally complex stamping involving both drawing and stretching suitable sheet ought to be characterized by high  $R$  and  $n$ .

## V. CONCLUSIONS

Sheets of various materials were securely clamped and stretched to failure by loading through solid punches. Strain measurements during stretching and observations of the eventual failures led to the conclusions:

1. Unstable plastic flow begins under conditions predicted by theory. If clamping is so secure that there is no drawing action, the intermediate principal strain increment is everywhere  $> 0$ . Then instability occurs by "diffuse necking"; it does not necessarily fix the punch-stretching limit, but rather tends only to increase the over-all non-uniformity of straining.
2. Stretching is terminated by ductile fracture, which is of special importance when localized necking is not allowed so that the flow is diffuse. A fracture criterion holding for the several annealed materials is an approximately constant value of the algebraically largest principal strain. Fracturing is closely related to details of microstructure and processing history.
3. Practical control of punch-stretching limits must be based principally upon control of the uniformity of strain distribution. Greater limits from more nearly uniform straining are obtained by more persistent strain hardening, lower punch-sheet interface friction, and smaller tool curvature. Some improvement may also be accomplished through increased fracture strain and regulation of plastic anisotropy.



4. In practical stamping failure-analysis, a knowledge of strain history would be helpful and may, in fact, be necessary.

5. An old conclusion is re-emphasized: Material suitable for generally complex stampings ought to be characterized by high values of properties such as the strain-hardening exponent,  $n$ , and the plastic anisotropy coefficient,  $R$ .

## REFERENCES

1. G. Sachs, W. Eisbein, W. Kuntze, and W. Linicus, "Spanlose Formung Der Metalle", Mitteilungen Der Deutschen Materialprüfungsanstalten, Sonderheft 16, (1931) p. 1.
2. H. W. Gillett, "Testing Deep Drawing Qualities of Sheet Metal", Metals and Alloys, Vol. 2, (1931) p. 214.
3. S. Y. Chung and H. W. Swift, "Cup-Drawing from a Flat Blank: Part I. Experimental Investigation, Part II. Analytical Investigation", Proceedings of the Institution of Mechanical Engineers, Vol. 165, (1951) p. 199.
4. S. Fukui, "Researches on the Deep Drawing Process", Scientific Papers of Tokyo Institute of Physical and Chemical Research, Vol. 34, (1938) p. 1422.
5. C. Arbel, "The Relation Between Tensile Tests and the Deep Drawing Properties of Metals", Sheet Metal Industries, Vol. 27, (1950) p. 921.
6. R. Pearce, "A Comparison Between the Swift Cupping Press and the Tensile Test for the Assessment of the Aluminum-Magnesium Series of Alloys for Deep Drawing and Pressing", Sheet Metal Industries, Vol. 30, (1953) p. 1077.
7. E. M. Loxley and P. Freeman, "Some Lubrication Effects in Deep Drawing Operations", Journal of the Institute of Petroleum, Vol. 40, (1954) p. 299.



8. D. A. Barlow, "The Formability of Aluminum Alloys", Engineering, Vol. 181, (1956) p. 329.
9. S. Fukui, H. Yuri, and K. Yoshida, "Analysis for Deep-Drawing of Cylindrical Shell Based on Total Strain Theory and Some Formability Tests", Aeronautical Research Institute, University of Tokyo, Report No. 332, Vol. 24 (1958) p. 43.
10. R. Pearce, "An Investigation into the Use of Swift Cupping Test for the Assessment of Steel Sheet for Cold Pressing", Sheet Metal Industries, Vol. 37, (1960) p. 523.
11. R. L. Whiteley, "The Importance of Directionality in Drawing Quality Sheet Steel", Transactions of American Society for Metals, Vol. 52, (1960) p. 154.
12. S. P. Keeler and W. A. Backofen, "Discussion to R. L. Whiteley, The Importance of Directionality in Drawing Quality Sheet Steel", Transactions of American Society for Metals, Vol. 52, (1960) p. 166.
13. O. H. Kemmis, "The Assessment of the Drawing and Forming Qualities of Sheet Metal by the Swift Cup-Forming Test", Sheet Metal Industries, Vol. 34, (1957) p. 203.
14. American Society for Metals Committee on Formability of Sheet Steel, "The Selection of Low-Carbon Steel Sheet for Formability", Metals Handbook, American Society for Metals, Novelty, Ohio, (1961).
15. H. W. Swift, "The Mechanism of a Simple Deep-Drawing Operation", Sheet Metal Industries, Vol. 31, (1954) p. 817.

16. W. T. Lankford, S. C. Snyder, and J. A. Bauscher, "New Criteria for Predicting the Press Performance of Deep Drawing Sheets", Transactions of the American Society for Metals, Vol. 42, (1950) p. 1197.
17. R. Hill, The Mathematical Theory of Plasticity, Clarendon Press, Oxford (1950).
18. R. Hill, "On Discontinuous Plastic States, with Special Reference to Localized Necking in Thin Sheets", Journal of the Mechanics and Physics of Solids, Vol. 1, (1952) p. 19.
19. H. W. Swift, "Plastic Instability Under Plane Stress", Journal of the Mechanics and Physics of Solids, Vol. 1, (1952) p. 1.
20. H. Ford, "Researches into the Deformation of Metals by Cold Rolling", Proceedings of the Institute of Mechanical Engineers, Vol. 159, (1948) p. 115.
21. G. A. Brewer and R. B. Glassco, "Determination of Strain Distribution by the Photo-Grid Process", Journal of Aeronautical Sciences, Vol. 9, (1941) p. 1.
22. J. A. Miller, "Improved Photogrid Techniques for Determination of Strain Over Short Gage Lengths", Proceedings for Experimental Stress Analysis, Vol. 10, No. 1, (1952) p. 29.
23. A. J. Durelli, E. A. Phillips, and C. H. Tsao, Introduction to the Theoretical and Experimental Analysis of Stress and Strain, McGraw-Hill Book Co., Inc., New York (1958).



24. G. T. van Rooyen and W. A. Backofen, "A Study of Interface Friction in Plastic Compression", International Journal of Mechanical Sciences, Vol. 1, (1960) p. 1.
25. R. L. Thorndike and E. P. Hagen, Measurement and Evaluation in Psychology and Education, John Wiley and Sons, Inc., New York (1955).
26. W. F. Brown, Jr. and G. Sachs, "Strength and Failure Characteristics of Thin Circular Membranes", Transactions of the American Society of Mechanical Engineers, Vol. 70, (1948) p. 241.
27. W. F. Brown, Jr. and F. C. Thompson, "Strength and Failure Characteristics of Metal Membranes in Circular Bulging", Transactions of the American Society of Mechanical Engineers, Vol. 71, (1949) p. 575.
28. P. B. Mellor, "Stretch Forming Under Fluid Pressure", Journal of the Mechanics and Physics of Solids, Vol. 5, (1956) p. 41.
29. H. C. Rogers, "The Tensile Fracture of Ductile Metals", Transactions of the Metallurgical Society of American Institute of Mining, Metallurgical, and Petroleum Engineers, Vol. 218, (1960) p. 498.
30. W. A. Backofen, "Metallurgical Aspects of Ductile Fracture", American Society for Metals Conference on Fracture of Engineering Materials, Rensselaer Polytechnic Institute, Troy, New York, August, 1959. To be published.

31. W. A. Backofen and B. B. Hundy, "Mechanical Anisotropy in Some Ductile Metals", Journal of the Institute of Metals, Vol. 81, (1953) p. 433.
32. W. A. Backofen, A. J. Shaler, and B. B. Hundy, "Mechanical Anisotropy in Copper", Transactions of American Society for Metals, Vol. 46, (1954) p. 655.
33. C. Crussard, D. Lajeunesse, and G. Pomey, "Influence De L'Anisotropie Des Toles Sur Leur Deformation Plastique En Sollicitations Uni Et Biaxiales", Paper Presented to International Deep Drawing Research Group and the Societe Francaise De Metallurgie, Paris (1960).



## APPENDIX A

## DETERMINATION OF CONDITIONS FOR INSTABILITY

All derivations are based on equations obtained from Hill.<sup>17,18</sup>

Definitions and Basic Equations

$\bar{\sigma}$  and  $\bar{\epsilon}$  are an invariant of the stress and strain tensor.

$$\bar{\sigma} = \left\{ \frac{1}{2} \left[ (\sigma_1 - \sigma_2)^2 + (\sigma_2 - \sigma_3)^2 + (\sigma_3 - \sigma_1)^2 \right] \right\}^{1/2} \quad (1-A)$$

For  $\sigma_3 = 0$  and  $X = \sigma_2/\sigma_1$ ,

$$\bar{\sigma} = \sigma_1 (1 - X + X^2)^{1/2}; \quad \bar{\sigma} = \sigma \text{ when } X = 0 \text{ in tension test} \quad (2-A)$$

Likewise

$$\bar{d\epsilon} = \left\{ \frac{2}{9} \left[ (d\epsilon_1 - d\epsilon_2)^2 + (d\epsilon_2 - d\epsilon_3)^2 + (d\epsilon_3 - d\epsilon_1)^2 \right] \right\}^{1/2} \quad (3-A)$$

Substituting

$$(d\epsilon_1 + d\epsilon_2 + d\epsilon_3) = 0 \quad (4-A)$$

$$\bar{d\epsilon} = \left[ \frac{2}{3} (d\epsilon_1^2 + d\epsilon_2^2 + d\epsilon_3^2) \right]^{1/2} \quad (5-A)$$

$$\bar{d\epsilon} = \frac{2d\epsilon_1}{2-X} (1 - X + X^2)^{1/2} = d\epsilon_1 \text{ for } X = 0 \quad (6-A)$$

The stress ratio  $X$  may be evaluated from the incremental strains.

From similarity of stress-strain circles

$$\frac{\sigma_1 - \sigma_2}{d\epsilon_1 - d\epsilon_2} = \frac{\sigma_2 - \sigma_3}{d\epsilon_2 - d\epsilon_3} = \frac{\sigma_3 - \sigma_1}{d\epsilon_3 - d\epsilon_1}$$

Combining with  $\sigma_3 = 0$ ,  $\sigma_2 = X\sigma_1$  and Eq. (4-A)

$$\frac{(1 - X)\sigma_1}{d\epsilon_1 - d\epsilon_2} = \frac{X\sigma_1}{d\epsilon_1 + 2d\epsilon_2} = \frac{\sigma_1}{2d\epsilon_1 + d\epsilon_2}$$

$$X = \sigma_2/\sigma_1 = \frac{d\epsilon_1 + 2d\epsilon_2}{2d\epsilon_1 + d\epsilon_2} = \frac{\epsilon_1' + 2\epsilon_2'}{2\epsilon_1' + \epsilon_2'} \quad (7-A)$$

where  $\epsilon_1'$  and  $\epsilon_2'$  are slopes of strain measurements; measured in this work as a function of pole height. For uniaxial tension  $d\epsilon_2/d\epsilon_1 = -1/2$  and  $X = 0$ , for plane strain  $d\epsilon_2 = 0$ ,  $X = 1/2$ , and balanced biaxial stress  $d\epsilon_1 = d\epsilon_2$ ,  $X = 1.0$ . Eq. (7-A) may be rewritten as:

$$\frac{d\epsilon_2}{d\epsilon_1} = \frac{2X - 1}{2 - X} \quad (8-A)$$

The strain increment equations, referred to principal axes of anisotropy, are

$$\begin{aligned} d\epsilon_1 &= d\lambda \left[ H (\sigma_1 - \sigma_2) + G (\sigma_1 - \sigma_3) \right] \\ d\epsilon_2 &= d\lambda \left[ F (\sigma_2 - \sigma_3) + H (\sigma_2 - \sigma_1) \right] \\ d\epsilon_3 &= d\lambda \left[ G (\sigma_3 - \sigma_1) + F (\sigma_3 - \sigma_2) \right] \end{aligned} \quad (9-A)$$



The ratio of the width to thickness strain obtained from a tension test is given as

$$R = d\epsilon_2/d\epsilon_3$$

Substituting Eq. (9-A) and  $\sigma_2 = \sigma_3 = 0$

$$R = H/G \text{ (for rotational isotropy)}. \quad (10-A)$$

Assuming plane stress ( $\sigma_3 = 0$ ) and rotational isotropy in the plane of the sheet ( $F = G$ ), Eqs. (9-A) are normalized by dividing through by  $G$  (arbitrarily setting  $G = 1$ ) and substituting Eq. (10-A)

$$\begin{aligned} d\epsilon_1 &= d\lambda \left[ (1 + R) \sigma_1 - R\sigma_2 \right] = \dot{\epsilon}_1 \\ d\epsilon_2 &= d\lambda \left[ -R\sigma_1 + (1 + R) \sigma_2 \right] = \dot{\epsilon}_2 \\ d\epsilon_3 &= d\lambda \left[ -(\sigma_1 + \sigma_2) \right] = \dot{\epsilon}_3 \end{aligned} \quad (11-A)$$

From Eqs.(11-A)

$$- d\epsilon_1/d\epsilon_2 = \frac{RX - (1 + R)}{(1 + R)X - R} \quad (12-A)$$

The yield condition is defined as

$$f = \left( \frac{G + H}{2} \right) \sigma_1^2 - H\sigma_1 \sigma_2 + \left( \frac{G + H}{2} \right) \sigma_2^2 = \bar{\sigma}^2$$

Substituting Eq. (10-A),

$$f = \left( \frac{1+R}{2} \right) \sigma_1^2 - R\sigma_1 \sigma_2 + \left( \frac{1+R}{2} \right) \sigma_2^2 = \bar{\sigma}^2 \quad (13-A)$$

$$\partial f / \partial \sigma_1 = (1+R) \sigma_1 - R\sigma_2, \quad \partial f / \partial \sigma_2 = (1+R) \sigma_2 - R\sigma_1 \quad (14-A)$$

$$\partial f / \partial \sigma_1 + \partial f / \partial \sigma_2 = \sigma_1 + \sigma_2 \quad (15-A)$$

$$\frac{\partial f / \partial \sigma_1}{\partial f / \partial \sigma_2} = \frac{\dot{\epsilon}_1}{\dot{\epsilon}_2} \quad (16-A)$$

$$\frac{\sigma_1 \partial f / \partial \sigma_1 + \sigma_2 \partial f / \partial \sigma_2}{\partial f / \partial \sigma_2} = \frac{\sigma_1 \dot{\epsilon}_1 + \sigma_2 \dot{\epsilon}_2}{\dot{\epsilon}_2} \quad (17-A)$$

Likewise, from Eqs. (16-A and 17-A)

$$\frac{\partial f / \partial \sigma_2}{\dot{\epsilon}_2} = \frac{\sigma_1 \partial f / \partial \sigma_1 + \sigma_2 \partial f / \partial \sigma_2}{\sigma_1 \dot{\epsilon}_1 + \sigma_2 \dot{\epsilon}_2} = \frac{\partial f / \partial \sigma_1 + \partial f / \partial \sigma_2}{\dot{\epsilon}_1 + \dot{\epsilon}_2} \quad (18-A)$$

### Angle of Localized Neck

The localized neck is oriented at an angle  $\alpha$  such that no extension occurs along the neck. Referring to Fig. 1A,  $d\epsilon_x$  is equal to zero; the only strain in the plane of the sheet is  $d\epsilon_y = d\ell_y / \ell_y$ . The change in length is resolved into two components,  $d\ell_1$  in the direction of  $\sigma_1$  and  $d\ell_2$  in the direction of  $\sigma_2$ .

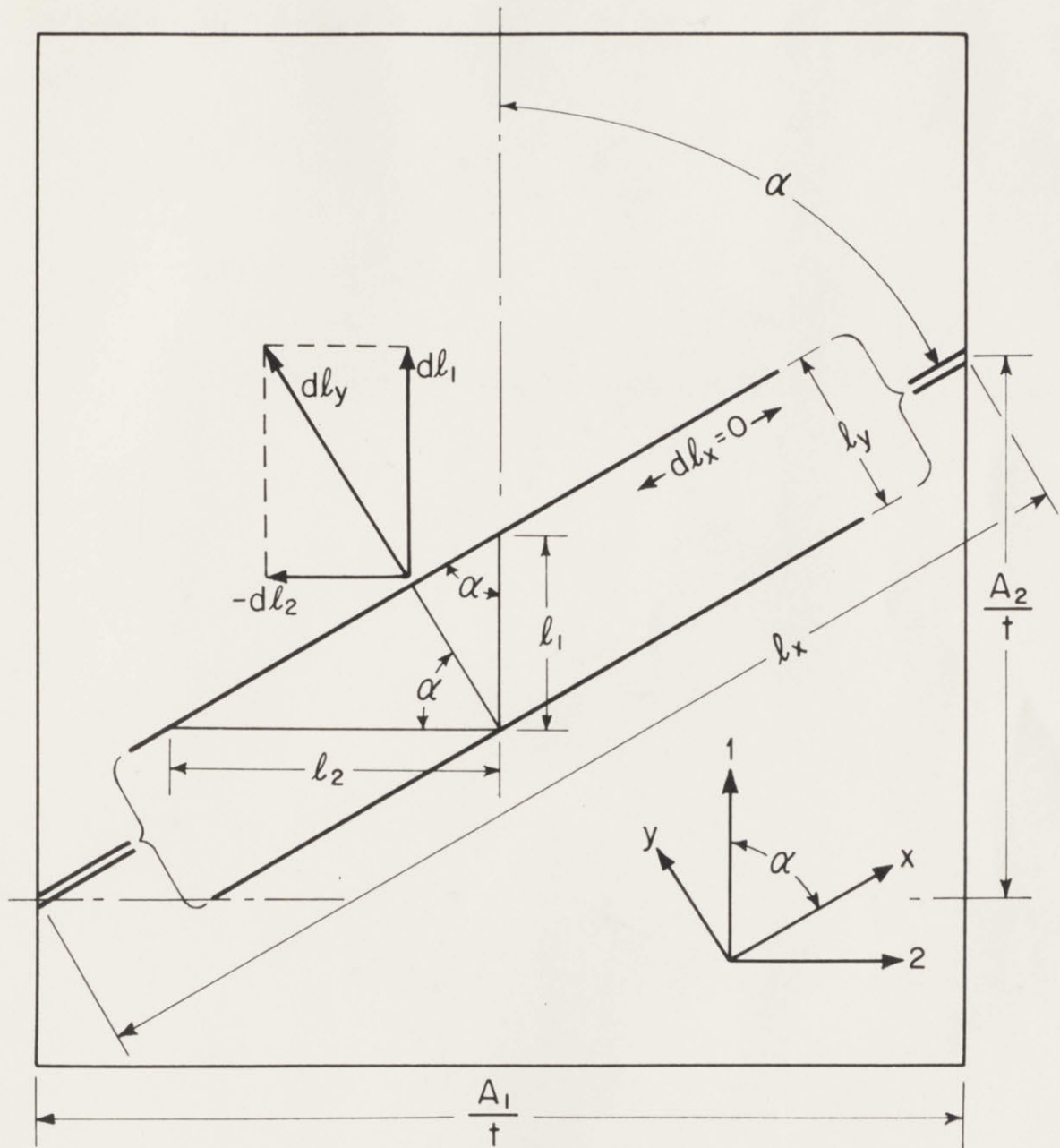


Fig. 1A - Components of Elongation of a Localized Neck in a Sheet Uniformly Loaded in Its Plane ( $\sigma_3 = 0$ ).



$$d\ell_1 = d\ell_y \sin \alpha$$

In addition, the gage length associated with  $d\ell_1$  now becomes

$$\ell_1 = \ell_y / \sin \alpha$$

$$d\epsilon_1 = d\ell_1 / \ell_1 = d\ell_y / \ell_y \sin^2 \alpha = d\epsilon_y \sin^2 \alpha \quad (19-A)$$

Likewise

$$d\epsilon_2 = d\epsilon_y \cos^2 \alpha \quad (20-A)$$

Combining Eqs. (19-A and 20-A)

$$\tan \alpha = \left( -d\epsilon_1 / d\epsilon_2 \right)^{1/2}$$

Substituting Eq. (12-A)

$$\tan \alpha = \left[ \frac{RX - (1 + R)}{(1 + R) X - R} \right]^{1/2} \quad (21-A)$$

With increased resistance to thinning ( $R > 1$ ),  $d\epsilon_2$  becomes more negative and  $\alpha$  decreases. For an isotropic material ( $R = 1$ ).

$$\tan \alpha = \left( \frac{X - 2}{2X - 1} \right)^{1/2} \quad (22-A)$$

For uniaxial tension test,  $X = 0$ ,  $\alpha = 54^\circ 44'$ . As the stress ratio increases,  $d\epsilon_2$  increases and  $\alpha$  increases. The limiting case is  $\alpha = 90^\circ$  ( $\tan \alpha = \infty$ ) when  $d\epsilon_2 = 0$ . For higher stress ratios,  $X$ ,  $d\epsilon_1 > d\epsilon_2 > 0$  and no direction of zero extension occurs in the plane of the sheet; now localized necking is not permitted. From Eq. (21-A)

$$(1 + R) X - R = 0 \text{ for } \tan 90^\circ = \infty$$

$$X_{\alpha = 90^\circ} = \frac{R}{1 + R} \quad (23-A)$$

Eq. (23-A) is plotted in Fig. 4.

#### Work Hardening Conditions

Without changing the load system, an increment of strain is allowed to occur. For instability, the increase in stress due to a reduction in area just balances the increase in stress-carrying capacity due to work hardening. Assuming the total amount of hardening to be a function of only the plastic work  $w$  per unit volume,

$$f(\sigma_1, \sigma_2) = F(w)$$

Rate of hardening is therefore

$$\frac{df(\sigma_1, \sigma_2)}{dt} = \frac{\partial f}{\partial \sigma_1} \cdot \frac{d\sigma_1}{dt} + \frac{\partial f}{\partial \sigma_2} \cdot \frac{d\sigma_2}{dt} = \dot{\sigma}_1 \frac{\partial f}{\partial \sigma_1} + \dot{\sigma}_2 \frac{\partial f}{\partial \sigma_2} \quad (24-A)$$

Change of total work equals

$$\frac{dF(w)}{dt} = \frac{dF(w)}{dw} \frac{dw}{dt} = F'(w) \cdot \dot{w}$$

$\dot{w}$  is increment of plastic work per unit time,

$$\dot{w} = \frac{dw_p}{dt} = \frac{\sigma_{ij} d\epsilon_{ij}^p}{dt} = \sigma_1 \frac{d\epsilon_1}{dt} + \sigma_2 \frac{d\epsilon_2}{dt}$$

$$\dot{w} = \sigma_1 \dot{\epsilon}_1 + \sigma_2 \dot{\epsilon}_2 \quad (25-A)$$

Combining Eqs. (24-A and 25-A)

$$\dot{\sigma}_1 \frac{\partial f}{\partial \sigma_1} + \dot{\sigma}_2 \frac{\partial f}{\partial \sigma_2} = (\sigma_1 \dot{\epsilon}_1 + \sigma_2 \dot{\epsilon}_2) F'(w)$$

$$F'(w) = \frac{\dot{\sigma}_1 \frac{\partial f}{\partial \sigma_1} + \dot{\sigma}_2 \frac{\partial f}{\partial \sigma_2}}{\sigma_1 \dot{\epsilon}_1 + \sigma_2 \dot{\epsilon}_2} \quad (26-A)$$

Diffuse Necking: The requirement of no change in external load

requires  $dP_1 = \sigma_1 dA_1 + A_1 d\sigma_1 = 0$

$$d\sigma_1/\sigma_1 = -dA_1/A_1 = d\epsilon_1, \quad \dot{\sigma}_1 = d\sigma_1/dt = \sigma_1 \dot{\epsilon}_1 \quad (27-A)$$

Likewise,

$$d\sigma_2/\sigma_2 = d\epsilon_2, \quad \dot{\sigma}_2 = \sigma_2 \dot{\epsilon}_2 \quad (28-A)$$



Substituting into Eq. (26-A)

$$F'(w) = \frac{\sigma_1 \dot{\epsilon}_1 \frac{\partial f}{\partial \sigma_1} + \sigma_2 \dot{\epsilon}_2 \frac{\partial f}{\partial \sigma_2}}{\sigma_1 \dot{\epsilon}_1 + \sigma_2 \dot{\epsilon}_2}$$

Combining with Eq. (16-A)

$$F'(w) = \frac{\sigma_1 (\frac{\partial f}{\partial \sigma_1})^2 + \sigma_2 (\frac{\partial f}{\partial \sigma_2})^2}{\sigma_1 \frac{\partial f}{\partial \sigma_1} + \sigma_2 \frac{\partial f}{\partial \sigma_2}} \quad (29-A)$$

Localized Necking: The change in cross sectional area due to deformation in the neck is  $dA_1 = l_x \sin \alpha dt$ , since  $dl_x = 0$  (Fig. 1-A).

$$\frac{d\sigma_1}{\sigma_1} = - dA_1/A_1 = - \frac{l_x \sin \alpha dt}{l_x \sin \alpha t} = - dt/t = - d\epsilon_3$$

Likewise,

$$\frac{d\sigma_2}{\sigma_2} = - d\epsilon_3$$

$$\dot{\sigma}_1/\sigma_1 = \dot{\sigma}_2/\sigma_2 = \dot{\epsilon}_1 + \dot{\epsilon}_2 = - \dot{\epsilon}_3 \quad (30-A)$$

Combining Eqs. (26-A and 30-A)

$$F'(w) = \frac{\dot{\sigma}_1}{\sigma_1} \frac{(\sigma_1 \frac{\partial f}{\partial \sigma_1} + \sigma_2 \frac{\partial f}{\partial \sigma_2})}{\sigma_1 \dot{\epsilon}_1 + \sigma_2 \dot{\epsilon}_2}$$

Substituting Eqs. (18-A and 30-A)

$$F'(w) = \frac{\dot{\sigma}_1}{\sigma_1} \frac{\partial f / \partial \sigma_1 + \partial f / \partial \sigma_2}{\dot{\epsilon}_1 + \dot{\epsilon}_2} = \partial f / \partial \sigma_1 + \partial f / \partial \sigma_2 \quad (31-A)$$

Evaluation of  $F'(w)$ :

$F(w) = f(\sigma_1, \sigma_2) = f(\bar{\sigma}, 0)$  in a uniaxial tension test,

$$F'(w) = \frac{dF(w)}{dw} = \frac{df(\bar{\sigma}, 0)}{dw} = \frac{df(\bar{\sigma}, 0)}{d\bar{\sigma}} \frac{d\bar{\sigma}}{d\bar{\epsilon}} \frac{d\bar{\epsilon}}{dw}$$

$$w = \int \bar{\sigma} d\bar{\epsilon}, \quad \frac{d\bar{\epsilon}}{dw} = 1/\bar{\sigma}$$

$$F'(w) = \frac{\partial f(\bar{\sigma}, 0)}{\partial \bar{\sigma}} \frac{1}{\bar{\sigma}} \frac{d\bar{\sigma}}{d\bar{\epsilon}} = \frac{\partial f(\bar{\sigma}, 0)}{\partial \bar{\sigma}} \beta \quad (32-A)$$

where  $\beta = \frac{1}{\bar{\sigma}} \frac{d\bar{\sigma}}{d\bar{\epsilon}} = 1/Z$  and decreases with increased straining along  $\bar{\sigma} - \bar{\epsilon}$  curve.  $\beta$  is equivalent to the  $r$  of Hill.<sup>18</sup>

$$\beta = \frac{n k \bar{\epsilon}^{n-1}}{k \bar{\epsilon}^n} = \frac{n}{\bar{\epsilon}}; \text{ as } n \text{ increases, therefore the value of}$$

$\bar{\epsilon}$  must likewise increase to obtain required value of  $\beta$ . From Eq. (14-A)

$$\frac{\partial f(\bar{\sigma}, 0)}{\partial \bar{\sigma}} = (1 + R) \bar{\sigma} = (1 + R) (1 - X + X^2)^{1/2}$$

$$F'(w) = \frac{(1 + R)}{Z/\bar{\sigma}} = \beta (1 + R) \bar{\sigma} \quad (33-A)$$

Final conditions for diffuse necking now become, combining (7-A, 14-A, and 29-A)

$$\beta = \frac{\sqrt{2} (1 + X) \left[ (1 + R)^2 - (1 + 4R + 2R^2) X + (1 + R)^2 X^2 \right]}{(1 + R) \left[ (1 + R) - 2RX + (1 + R) X^2 \right]^{3/2}} \quad (34-A)$$

For isotropic material

$$\beta = 1/Z_d = \frac{(1 + X)(4 - 7X + 4X^2)}{4(1 - X + X^2)^{3/2}}$$

Likewise, for localized necking, combining Eqs. (7-A, 14-A, and 31-A)

$$\beta = \frac{1 + X}{(1 + R) \left[ \left( \frac{1 + R}{2} \right) - RX + \left( \frac{1 + R}{2} \right) X^2 \right]^{1/2}} \quad (36-A)$$

For isotropic material

$$\beta = 1/Z_l = \frac{1 + X}{2(1 - X + X^2)^{1/2}} \quad (37-A)$$

The respective strains  $\bar{\epsilon}_d^*$  and  $\bar{\epsilon}_l^*$  are determined by the tangent construction of Fig. 1. The principal components of strain are then determined by Eq. (6-A).

Condition for diffuse necking (Eq. 27A) is

$$\frac{d\sigma_1}{\sigma_1} = d\epsilon_1 = -\frac{dA}{A}$$



and for localized necking (Eq. 30-A), due to restricted flow,

$$\frac{d\sigma_1}{\sigma_1} = - d\epsilon_3 = \frac{d\epsilon_1}{2} = - 1/2 \frac{dA}{A}$$

At load maximum,  $dP = 0$ ,  $\frac{d\sigma}{\sigma} = - dA/A$ . Conditions for diffuse necking are thus satisfied at load maximum. However, further straining is required before  $d\sigma_1/\sigma_1 = - 1/2 dA/A$ . Therefore  $Z_l > Z_d$ , except when  $d\epsilon_2 = 0$  and both modes of necking are identical.

## APPENDIX B

## DETAILS OF SPECIMEN PREPARATION AND TESTING APPARATUS

Specimen PreparationMachining:

- a. Circles of 8.2 in. diameter were scribed in the center of the sheet material. Stock for steel specimens was obtained in the form of 10 in. squares; stock for other specimens was either 6 ft. by 1 ft. or 6 ft. by 2 ft. sheets.
- b. Circles were rough cut on a band saw.
- c. Rough specimens were grouped in packs of 5 to 7 and placed on a lathe between the chuck face and a face plate held by a dead center. Soft materials were sandwiched between hard materials. Discs were turned on the lathe to a finished diameter dimension of  $8.000 + .000/- .001$  inches.

Grid Application:

- a. One side of the disc was prepared for photographing by cleaning the surface with 240 emery; this was followed by a soap cleaning, water rinse, and an acetone bath.
- b. Photoengraving cold top enamel<sup>21,22</sup> was brushed on the disc to wet the surface. Cold top enamel was then liberally flowed over the surface of the tilted disc, and allowed to drain from the bottom. The specimen was rotated, removing excess enamel from the bottom edge of the

disc with a brush until the enamel was dry. Unused enamel should be discarded after one year, as it loses its sensitivity.

c. A negative was made from graph paper having the desired grid pattern (negative was transparent with black grid lines). The negative was placed, emulsion side down, on top of the coated specimen surface and centered by alignment of grid lines and edge of specimen. A glass plate was laid over the negative and was clamped to the disc, thus permitting complete contact between specimen and negative.

d. The specimen and negative were exposed to an arc light. Exposure time was dependent upon the strength of the arc, distance to arc, thickness of enamel layer, and increased with ageing of the enamel. The specimen had to be exposed and developed within 1-1/2 hours after coating with enamel, although 1/2 hour was found to be best.

e. After the negative and glass plate had been removed from the specimen following exposure, the specimen was immersed in cold top developer. When the grid lines became apparent, the disc was rinsed under a forceful water stream from a faucet. The grid lines were purple, while the enamel from the unexposed area had floated away. Selective brushing was required to remove sticking flakes of unexposed enamel.

f. Grid was permanently set by the application of slight heat (uncomfortable to touch) or by letting the specimens stand for several days. J. A. Miller<sup>22</sup> of the National Bureau of Standards has shown that a properly applied grid will withstand a strain of 110% before separation from the metal surface.



g. Discs were cleaned with weak acid to remove traces of blue developer staining the bare metal and to slightly etch the image of the grid into the discs.

#### Final Preparation:

a. The 4 in. diameter center area of the reverse side of the disc was cleaned and polished with 4/0 emery. Outer ring of 4 in. to 8 in. diameter was roughened on a grinding wheel for better clamping by the holddown ring.

b. Entire specimen was cleaned with soap solution and water rinse. Area of punch contact was again cleaned with acetone and a clean cloth just before testing.

c. For lubrication an aqueous dispersion of Teflon was brushed evenly on the 4 in. center and allowed to dry. During interrupted testing the lubricant was removed by a clean cloth and acetone, specimen cleaned with acetone, and a new, smooth coat of lubricant reapplied before reinsertion into the subpress for the next stage of testing. Tool, die, and specimen were thoroughly cleaned with acetone between every cycle of interrupted loading.

#### Apparatus and Test Procedure

A subpress (Fig. 3) was designed for insertion in a 200,000 lb. Tate-Emery Baldwin tensile testing machine.

The subpress was composed of three groups of parts: (1) die ring (B) and support system affixed to bed of testing machine by clamps, (2) hold-down and ram guidance system (C), aligned to die support system by pins, and (3) punch (F) and ram system, affixed to machine crosshead.

Die ring (B) was supported in the die holder; a circular die opening with an edge radius of  $3/8$  in. was used for all tests.

Clearance between punch and edge of die hole was equal to specimen thickness plus 35% of specimen thickness. The die ring was depressed one-half of specimen thickness below the face of the die holder; this permitted centering and holding of the specimen.

Specimens (A) were placed on the die (B), grid side away from punch. A flat ring, sandblasted on one side, was placed on the specimen to further insure against slippage. The holddown ring (C), placed on top of the holding ring, was aligned by guide pins, and acted as a guide tube for punch and ram.

Supports were placed between the crosshead and spring loading plate (E). As the bed of the press was driven upwards, the Belleville washer springs (D) were compressed to a pre-determined load. Each spring has a plateau in the load deflection curve at 5,500 lbs.; six springs stacked in parallel (additive load) therefore, had a load plateau at 33,000 lbs. for constant holddown load. The nuts were tightened (until deflection on load indicator noted) to keep the springs compressed. Spring loading plate was then unloaded and supports removed.



A ram with interchangeable punch (F) was lowered to contact specimen and loading applied; autographic records of load were made. The shaft connecting ram to the crosshead was permitted to rotate independently of the ram, thus preventing any tilting and jamming of the ram by crosshead movement. Ram speed was about 0.1 in./min. Depth of ram was roughly determined by the attached ram pacer unit. Accurate pole height measurements were made after removal of the specimen from the subpress, using a depth gage to measure distance from clamped rim to pole.

Blank was deformed a desired amount and punch withdrawn. Springs were unloaded in a manner reverse to loading. Specimen was then removed for measurement, cleaning and relubrication.



## APPENDIX C

## ADDITIONAL SAMPLING OF STRAIN HISTORY DATA

The data presented here represent a sampling of elements from each test to include failure and surrounding elements. The statistical test was applied to this information.

TABLE IA  
STRAIN HISTORY OF VARIOUS ELEMENTS FROM EACH CUP

Test	$r_o$ , in.	Region I		I-II Discontinuity					Region II		Terminal <sup>+++</sup>	
		$\epsilon'_r$	X	$h^*$	$\bar{\epsilon}^*$	$\bar{\epsilon}_d^*$	$\epsilon_r^*$	$\epsilon_l^*$	$\epsilon'_r$	X	$\bar{\epsilon}$	$\epsilon_r$
Al (1/2 h)-HT Max. h = 1.00 in. <sup>+</sup>	0.25	0.22	0.95	0.60	0.21	0.19	0.12	0.10	0.27	0.87	0.39	0.23
	0.35	0.24	0.94	0.60	0.22	0.19	0.12	0.10	0.38	0.81	0.47	0.29
	0.40 <sup>++</sup>	0.24	0.96	0.60	0.23	0.19	0.11	0.10	0.43	0.77	0.48	0.30
	0.50	0.23	0.97	0.60	0.20	0.19	0.11	0.10	0.40	0.86	0.46	0.27
	0.60	0.20	0.93	0.60	0.19	0.19	0.10	0.10	0.30	0.94	0.41	0.22
	0.70	0.16	0.89	0.73	0.21	0.18	0.10	0.10	0.30	0.92	0.36	0.18
Al (1/2 h)-HD Max. h = 0.82 in. <sup>+</sup>	0.40	0.15	0.80	0.70	0.16	0.15	0.10	0.10	0.24	0.70	0.20	0.13
	0.50	0.18	0.80	0.66	0.17	0.15	0.10	0.10	0.43	0.64	0.30	0.18
	0.60 <sup>++</sup>	0.21	0.79	0.63	0.17	0.14	0.10	0.09	0.60	0.62	0.31	0.22
	0.70	0.21	0.87	0.65	0.17	0.17	0.10	0.10	0.64	0.66	0.38	0.21
	0.80	0.21	0.93	0.69	0.18	0.18	0.10	0.10	0.38	0.77	0.29	0.15
	0.90	0.19	0.93	0.82	0.18	0.18	0.10	0.10	0.44	0.72	0.25	0.12
Cu(s)-HT Max. h = 1.77 in. <sup>+</sup>	1.10	0.19	1.00	1.65	0.39	0.46	0.23	0.23	1.00	0.63	0.51	0.37
	1.20 <sup>++</sup>	0.23	0.97	1.64	0.41	0.46	0.25	0.24	1.00	0.63	0.56	0.38
	1.40	0.23	0.82	1.67	0.39	0.44	0.26	0.29	0.62	0.69	0.46	0.31

<sup>+</sup> Height at fracture in the "failure element".

<sup>++</sup> Failure element.

<sup>+++</sup> The values in this column are associated with the various elements when fracture occurs in the "failure element".

TABLE IA (Continued)

Test	$r_o, \text{in.}$	Region I		I-II Discontinuity					Region II		Terminal <sup>+++</sup>	
		$\epsilon'_r$	X	$h^*$	$\bar{\epsilon}^*$	$\bar{\epsilon}_d^*$	$\epsilon_r^*$	$\epsilon_l^*$	$\epsilon'_r$	X	$\bar{\epsilon}$	$\epsilon_r$
Cu(s)-ET Major Axis Max. h = 1.47 in. <sup>+</sup>	1.20	0.31	0.91	1.42	0.44	0.46	0.28	0.27	--	--	0.47	0.30
	1.40	0.32	0.92	1.30	0.36	0.46	0.24	0.26	0.76	0.71	0.52	0.38
	1.60 <sup>++</sup>	0.41	0.82	1.30	0.44	0.44	0.29	0.29	0.90	0.67	0.60	0.44
	1.70	0.83	0.82	1.35	0.42	0.44	0.29	0.29	0.65	0.72	0.52	0.38
Al(s)-HT Max. h = 1.57 in. <sup>+</sup>	0.70	0.19	0.89	None	None	0.38	None	0.23	None	None	0.38	0.22
	0.80	0.22	0.86	1.56	0.36	0.36	0.22	0.22	--	--	0.41	0.25
	1.00	0.25	0.80	1.30	0.32	0.33	0.21	0.22	0.49	0.71	0.50	0.33
	1.20 <sup>++</sup>	0.30	0.83	1.30	0.32	0.34	0.22	0.22	0.65	0.60	0.59	0.41
	1.40	0.28	0.90	1.38	0.34	0.39	0.22	0.22	0.50	0.75	0.47	0.32
	1.50	0.25	0.97	1.56	0.36	0.43	0.23	0.23	--	--	0.39	0.26
Al(s)-HD Max. h = 1.30 in. <sup>+</sup>	0.90	0.15	0.82	None	None	0.34	None	0.22	None	None	0.26	0.18
	1.10	0.28	0.73	1.18	0.31	0.30	0.20	0.20	0.35	0.69	0.34	0.25
	1.30 <sup>++</sup>	0.30	0.72	1.18	0.29	0.29	0.20	0.20	0.88	0.58	0.41	0.32
	1.50	0.28	0.73	None	None	0.29	None	0.20	None	None	0.26	0.20
Al(s)-ET Major Axis Max. h = 1.32 <sup>+</sup>	1.20	0.24	1.00	None	None	0.46	None	0.24	None	None	0.37	0.23
	1.40	0.32	0.89	1.16	0.33	0.38	0.22	0.22	0.43	0.82	0.43	0.30
	1.60 <sup>++</sup>	0.51	0.83	1.04	0.32	0.35	0.23	0.22	0.80	0.73	0.53	0.36

+ Height at fracture in the "failure element".

++ Failure element.

+++ The values in this column are associated with the various elements when fracture occurs in the "failure element".



TABLE IA (Continued)

Test	$r_o, \text{in.}$	Region I		I-II Discontinuity					Region II		Terminal <sup>+++</sup>	
		$\epsilon'_r$	X	$h^*$	$\bar{\epsilon}^*$	$\bar{\epsilon}_d^*$	$\epsilon_r^*$	$\epsilon_l^*$	$\epsilon'_r$	X	$\bar{\epsilon}$	$\epsilon_r$
Steel-HT Max. h = 2.10 in. <sup>+</sup>	0.75	0.13	0.93	None	None	0.52	None	0.29	None	None	0.41	0.23
	1.00	0.17	0.86	2.05	0.46	0.50	0.29	0.31	0.44	0.66	0.59	0.32
	1.25 <sup>++</sup>	0.23	0.82	2.05	0.48	0.49	0.31	0.32	0.55	0.65	0.57	0.41
	1.50	0.22	0.82	2.05	0.41	0.49	0.29	0.32	0.58	0.64	0.44	0.32
Steel-HD Max. h = 1.84 in. <sup>+</sup>	1.60	0.38	0.61	None	None	0.41	None	0.32	None	None	0.36	0.30
	1.70 <sup>++</sup>	0.44	0.50	1.83	0.35	0.35	0.31	0.31	--	--	0.37	0.33
Steel-CT Max. h = 1.42 in. <sup>+</sup>	0.10	0.25	0.91	None	None	0.52	None	0.30	None	None	0.44	0.26
	0.30	0.28	0.96	1.35	0.51	0.52	0.28	0.28	0.86	0.69	0.58	0.33
	0.45 <sup>++</sup>	0.32	0.99	1.28	0.51	0.52	0.28	0.27	1.30	0.66	0.74	0.46
	0.60	0.24	0.92	None	None	0.52	None	0.30	None	None	0.51	0.28
Brass(s)-HT Max. h = 2.20 in. <sup>+</sup>	1.20	0.18	0.88	None	None	0.63	None	0.38	None	None	0.48	0.32
	1.40	0.22	0.83	None	None	0.61	None	0.38	None	None	0.51	0.36
	1.60 <sup>++</sup>	0.23	0.80	None	None	0.60	None	0.39	None	None	0.51	0.39
Brass(s)-CT Max. h = 1.96 in. <sup>+</sup>	0.25	0.23	0.99	1.91	0.66	0.66	0.34	0.33	0.40	0.80	0.70	0.36
	0.45 <sup>++</sup>	0.35	0.85	1.72	0.63	0.62	0.38	0.38	0.44	0.79	0.77	0.46
	0.65	0.26	0.97	None	None	0.66	None	0.34	None	None	0.63	0.36

+ Height at fracture in the "failure element".

++ Failure element.

+++ The values in this column are associated with the various elements when fracture occurs in the "failure element".

APPENDIX D  
INSTABILITY IN HYDRAULIC BULGE TESTS

The pressure maximum is taken as onset of instability in the bulge test.<sup>26</sup> The bulge approximates a sphere at the pole; therefore, the stress is  $\sigma = Pr/2t$ . Differentiating,

$$d\sigma/\sigma = dP/P + dr/r - dt/t \quad (38-A)$$

At the pressure maximum  $dP/P = 0$ , and Eq. (38-A) reduces to

$$\frac{d \ln \sigma}{d\epsilon_3} = \frac{d \ln r}{d\epsilon_3} - 1 \quad (39-A)$$

The onset of theoretical instability is determined by graphical solution of Eq. (39-A), using experimental values of  $\sigma$ ,  $\epsilon$ , and  $r$  obtained at the pole of the bulge. A discontinuity is noted in the strain of all elements removed from the pole when plotted as a function of pole strain,<sup>27</sup> indicating an increased rate of strain at the pole. This increased rate of straining also occurs in the radial strain history of the pole element plotted in Fig. 2A from the data of Brown and Thompson;<sup>27</sup> the strain history parallels that found in punch stretching. The values of theoretical instability strain are indicated by  $\epsilon_T^*$ , and agree with the strain discontinuity. A blister forms at the pole at instability. The decrease in radius of curvature reduces the stress at that location, straining ceases on the blister, and the area of necking spreads and becomes "diffuse".<sup>27</sup> Thus, considerable flow can occur after onset of instability.

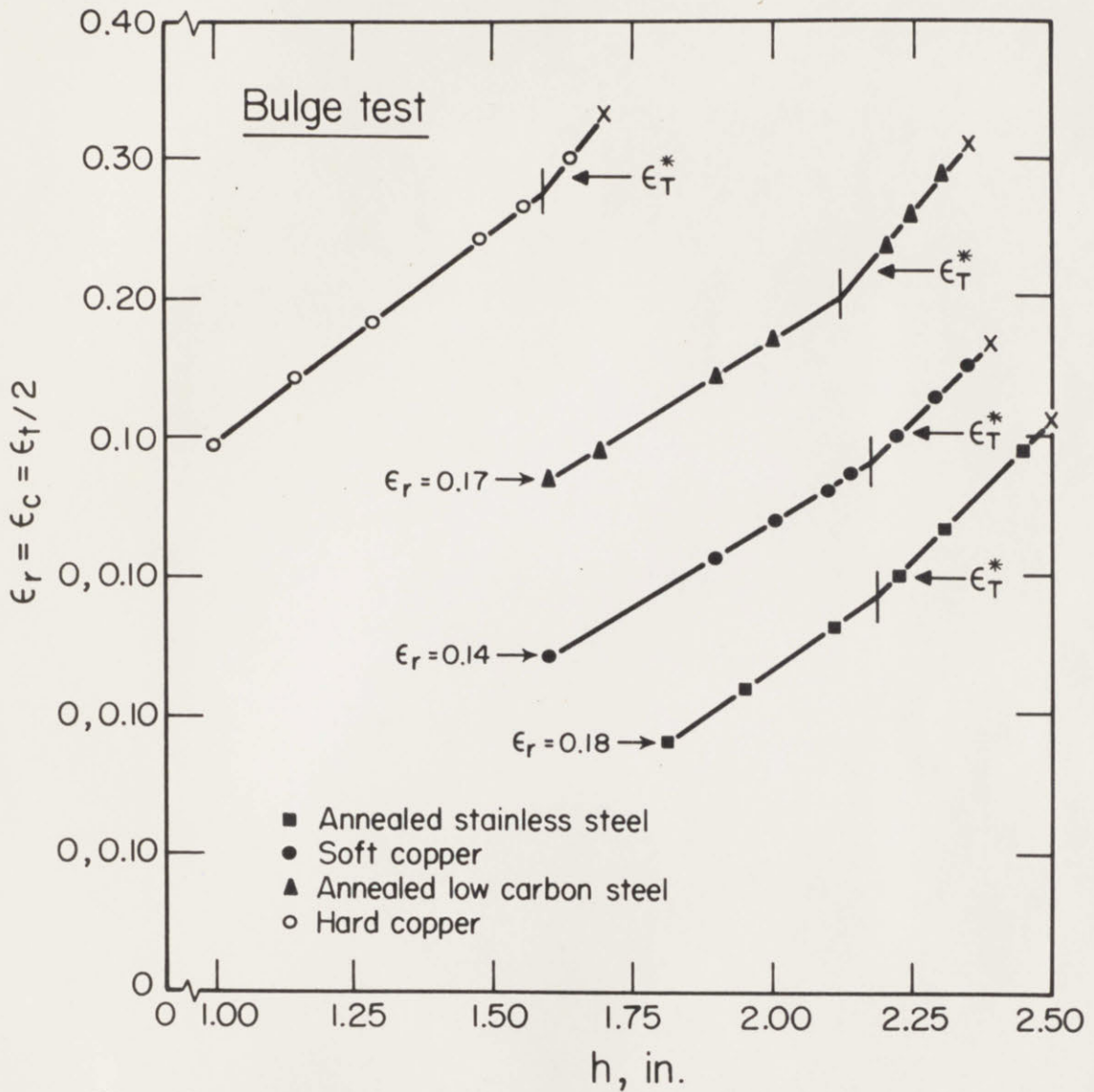


Fig. 2A - Strain vs. Pole Height for Various Materials in Bulge Testing. Data were replotted from Brown and Thompson<sup>27</sup> to show straining behavior similar to punch stretching. Strain predicted for onset of instability is indicated by  $\epsilon_T^*$ .



APPENDIX E  
FRACTURE EXAMINATION

Specimens from tensile strips and sheets stretched over rigid punches were sectioned perpendicular to the line of fracture and nickel plated. Plated specimens were mounted so as to view the thickness profile and then polished. Profile measurements of the area surrounding the fracture site were made with a microscope and calibrated eye-piece. It was found that 1 mm distance (Table IV) was sufficient to extend beyond the localized neck. Some of the change in profile of the stretched sheets, where localized necking is not permitted, may be attributed to the strain gradient occurring between the pole and rim.

An enlargement of the crack forming in the hard copper (Fig. 19) is shown in Fig. 3A.

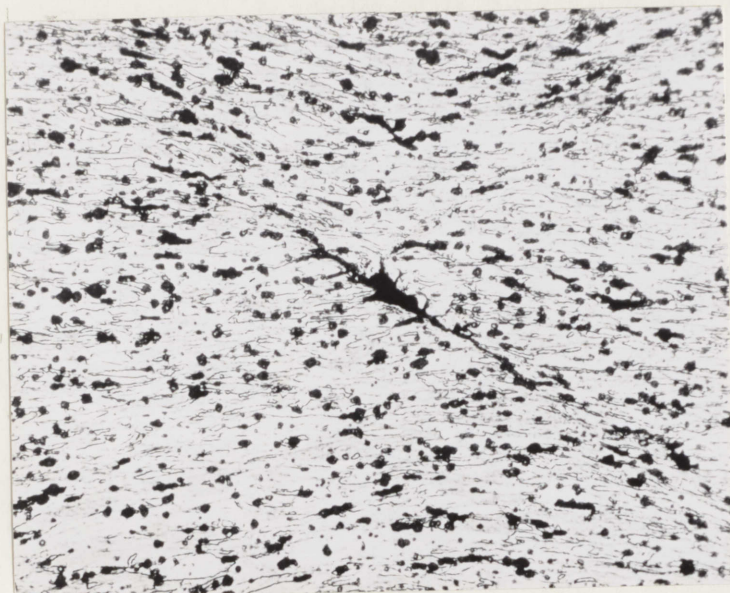


Fig. 3A - Enlargement of Crack Found Along Shear Band in Hard Copper (HT). Ammonium Persulfate Etch, X300.

## SUGGESTIONS FOR FUTURE WORK

The following areas are suggested for further study of sheets stretched over rigid punches.

1. Studies on the interaction of radial drawing and punch stretching. Variable amounts of clamping would allow transition from one extreme of stretching to the other extreme of radial drawing. The effect of lubrication, punch design, and material properties should be determined as the transition is made.

2. Develop equations describing flow of material being stretched over rigid tools. The equations could predict optimum set of material and processing variables to attain maximum stretching limits. Such equations might be developed first for a simple shape such as a hemispherical punch and compared with experimental strain distributions. It would be instructive to relate these equations to those of radial drawing, and attempt to establish theoretical limits for radial drawing with a hemispherical punch.

3. Studies of strain history in complex commercial stampings. Measurement of strain history from partial stampings should be made to test the accuracy with which proximity to failure might be ascertained, and correlate this with shop practice. Specification of quality control limits for material and processing variables should be attempted.



## BIOGRAPHICAL NOTE

Stuart Philip Keeler was born in Wausau, Wisconsin, on September 1, 1934. After graduating from Wausau High School, he was enrolled at Ripon College, Wisconsin from 1952 to 1955 and at the Massachusetts Institute of Technology from 1955 to 1957. In 1957 he graduated with the degree of Bachelor of Arts from Ripon College and Bachelor of Science from the Massachusetts Institute of Technology. He enrolled as a graduate student in the Department of Metallurgy at the Massachusetts Institute of Technology in 1957 and was appointed National Steel Fellow.

He was elected to Tau Beta Pi, Phi Beta Kappa and Sigma Xi, and is a member of the American Institute of Mining, Metallurgical, and Petroleum Engineers.